

Friedrich-Schiller-University Jena

Faculty for Chemistry and Earth Sciences

Institute for Inorganic and Analytical Chemistry &

Max-Planck-Institute for Chemical Ecology, Dpt. Natural Product Biosynthesis



**Structural Elucidation and Studies Towards the Biosynthesis of a Bis-
Indole Alkaloid in *Tabernaemontana donnell-smithii***

Bachelor Thesis

To gain the academic grade as a
Bachelor of Science in the Study Program *Chemistry* (B. Sc.)

Submitted by

Philippe René Meisinger

Born in Arnstadt, the 15.09.1997

Jena, September 2020

First Consultant: Dr. Thomas Wichard

Second Consultant: jun.-Prof. Ivan Vilotijevic

Selbständigkeitserklärung

Hiermit versichere ich, dass ich die vorliegende Arbeit selbstständig verfasst und keine anderen als die angegebenen Quellen und Hilfsmittel benutzt habe, alle Ausführungen, die anderen Schriften wörtlich oder sinngemäß entnommen wurden, kenntlich gemacht sind und die Arbeit in gleicher oder ähnlicher Fassung noch nicht Bestandteil einer Studien- oder Prüfungsleistung war.

Ort, Datum

Unterschrift

Tab. 0: Compound List

number	compound
1	morphine
2	quinine
3	strychnine
4	coronaridine
5	tabersonine
6	vobasine
7	(3 <i>R</i>)-tabernaelegantinal E
8	tabernaengelantine D
9	(3 <i>R</i>)- tabernaengelantine D
10	vinblastine
11	ervatensine A
12	ervatensine B
13	cononphyllin
14	tryptophan
15	secologanin
16	tryptamine
17	strictosidine
18	ajmalin
19	camptohtecin
20	strictosidine hemiacetal
21	strictosidine dialdehyde
22	4,12-dehydrocorynanthine
23	4,12-dehydrogeissoschizine
24	geissoschizine
25	rhazimal
26	dehydropreakkumanicine
27	preakkumamicine
28	stemmadenine
29	stemmadenine actetat
30	dihydroprecondylocarpine
31	ehydrosecodine
32	angryline
33	angustilongine C
34	14,15-dehydrotetrastachyne
35	14,15-dehydrotetrastachynine
36	catharanthine

TABLE OF CONTENTS

1 Introduction	1
1.1 General remarks on bis-indole alkaloids	1
1.2 Biosynthesis of aspidosperma and iboga scaffolds	3
1.3 Aim of this work	6
2 Materials and Methods	7
2.1 NMR Analysis.....	7
2.2 Substrate feeding to <i>T. donell-smithii</i>	7
2.3 Root microsome preparation	7
2.4 Activity screening for microsomes.....	8
3 Results	9
3.1 Structural characterisation of the isolated BIA of <i>T. donell-smithii</i>	9
3.2 Substrate feeding to <i>T. donell-smithii</i>	24
3.3 Microsome assay	26
4 Discussion	31
4.1 Structural characterization of the isolated BIA of <i>T. donell-smithii</i>	31
4.2 Substrate feeding to <i>T. donnell-smithii</i>	32
4.3 Microsome assay	32
4.3 Outlook	33
5 Conclusion.....	34
6 Zusammenfassung.....	35
7 Acknowledgement	35
8 References	35
Appendix	37

1 Introduction

1.1 General remarks on bis-indole alkaloids

Plants have been used for thousands of years for their medicinal and poisonous properties.^[1] Initially people did not know about the molecules present in these plants that are responsible for the biological activities. However, with the dawn of chemistry as a scientific discipline, an awareness arose about the materialistic basis of our world. In 1805 the first alkaloid was isolated in its pure form: morphine (**1**) (fig. 1).^[2] The isolation was done by the German chemist Friedrich Wilhelm Sertürner from opium; this was the first step towards an understanding of plant alkaloid constituents and laid the groundwork for their medical application. Since then the number of identified alkaloids has exploded, as well as their use in medicine. For example **1** has been used as a painkiller for centuries^[3], quinine (**2**) is in use as an anti-malaria drug^[4] as well as strychnine (**3**), which is used in ayurvedic medicine to treat anorexia, fever or to stimulate digestion but also in modern medicine as a radioactive marked **3** to trace glycine receptors.^[5]

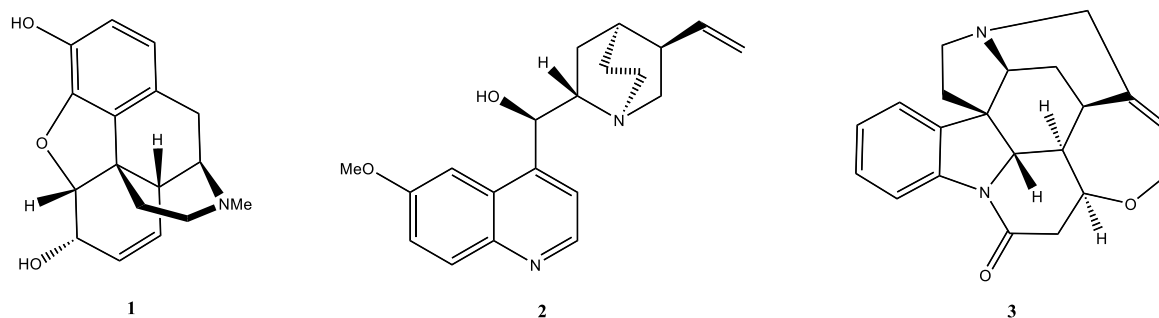


Fig. 1: Structures of morphine (**1**), quinine (**2**) and strychnine (**3**).

Alkaloids display huge structural variety. One special class of alkaloids are bis-indole alkaloids (BIA). They consist of two monoterpenoid indole alkaloids (MIA), which are covalently linked to form a dimer. MIAs are natural products that have their biosynthetic origin in the amino acid tryptophan (**14**) and the monoterpene secologanin (**15**) (see chapter 1.2). A great structural variety arises just by the connection of different MIA skeletons, most commonly the iboga, aspidosperma or vobasine scaffolds, represented by coronaridine (**4**), tabersonine (**5**) and vobasine (**6**) respectively (fig. 2), which can be connected in many different ways.^[6]

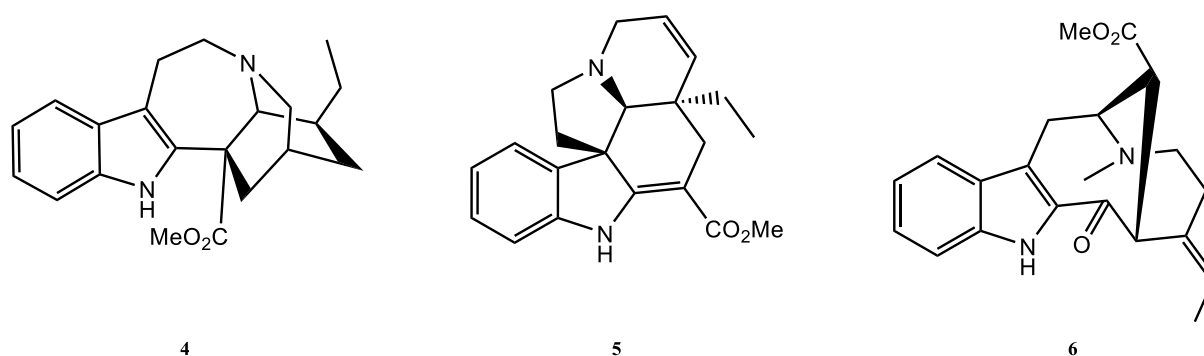


Fig.2: Scaffolds of iboga- (**4**), aspidosperma-(**5**) and vobasine-(**6**) MIAs

Using different MIA scaffolds as monomers is only the starting point for BIA structural diversity. The same building blocks can be connected in many different ways, as seen in (*3'R*)-tabernaegantinal E (**7**) and tabernaegantine D (**8**) (fig. 3). Compound **7** is connected between C-3 of the vobasine monomer and C-12' of the coronaridine monomer, whereas **8** is connected between C-3 and C-10'. BIAs can also be further modified, by hydroxylations, methylations or rearrangements. This is easily visible in the comparison of **8** and (*3'R*)-hydroxytabernaegantine D (**9**) (fig. 2), which differ only in oxidation of the coronaridine monomer.

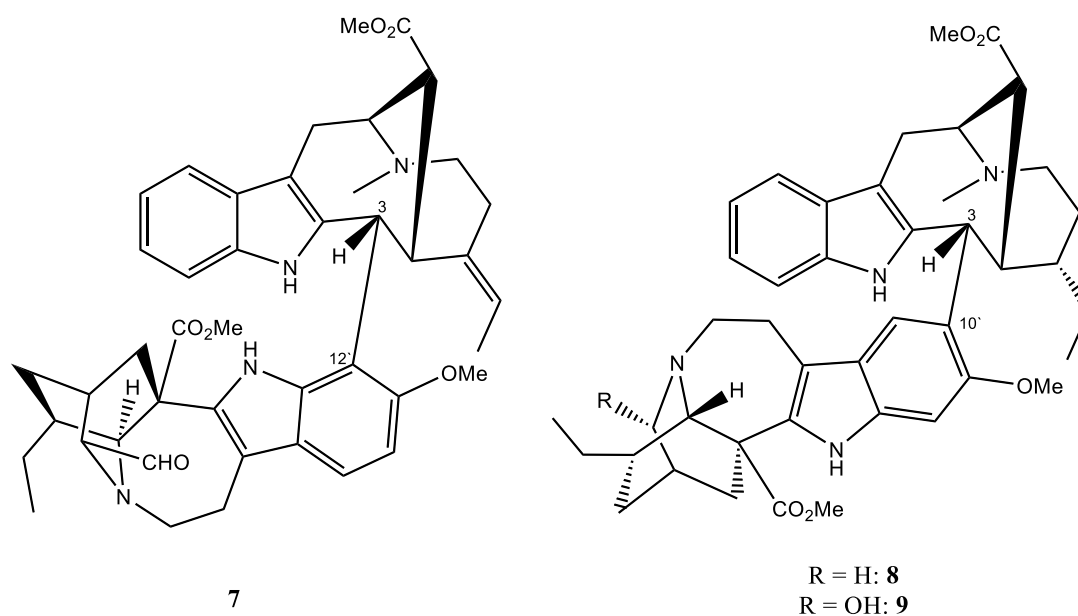


Fig. 3: Structures of (*3'R*)-tabernaegantinal E (**7**), tabernaegantine D (**8**) and (*3'R*)-hydroxytabernaegantine D (**9**)

BIAs also show a wide range of biological activities. One of the most prominent examples is vinblastine (**10**) (fig. 4), a vinca-alkaloid isolated from *Catharantus roseus*. Vinblastine is used in chemotherapy to treat a variety of cancers, including breast and bone cancer.^[7] The mode of action is well understood for vinblastine: it binds specifically to the microtubules involved in cell division and thereby prevents their polymerization.^[7,8] Through this inhibition of cell proliferation, cells undergo apoptosis, blocking endothelial proliferation, an essential step in angiogenesis, at concentrations as low as 0.1 to 1.0 pmol/L.^[9]

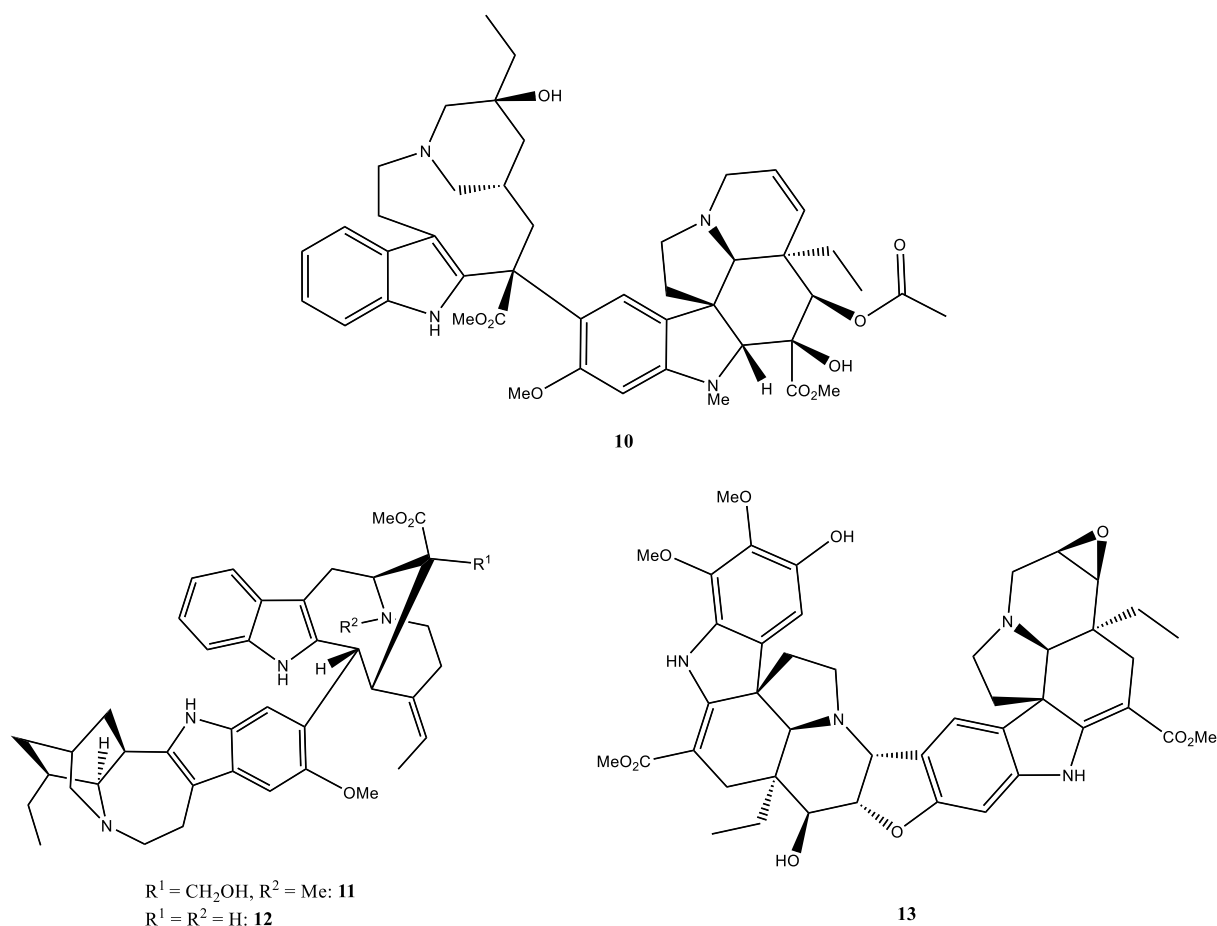


Fig. 4: Structures of vinblastine (**10**), ervatensine A and B (**11** and **12**) and conophyllin (**13**)

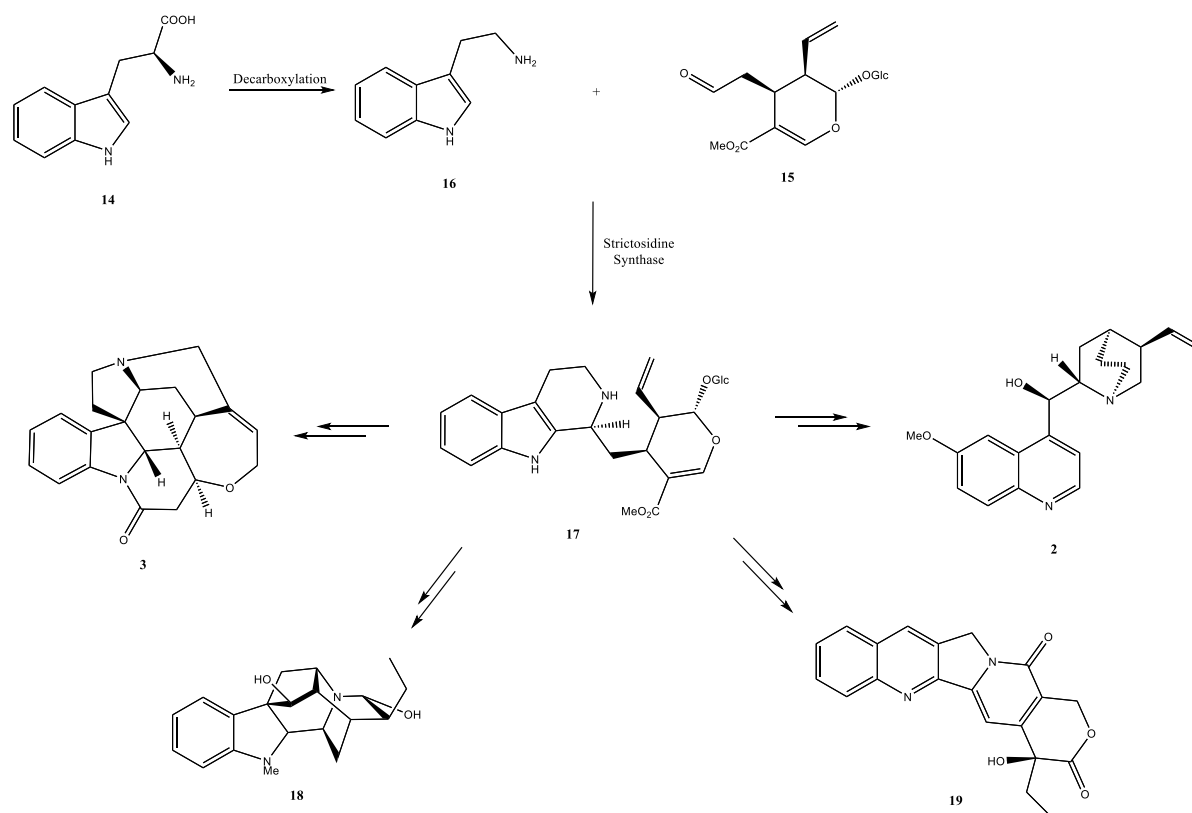
In search of new BIAs that may serve as good drug leads, alkaloid-producing plant families are an excellent point to start. In the last decades, it was shown that *Tabernaemontana* species produce many BIAs. Examples are **7-9**, which were isolated from *T. sissilifolia* in 2012,^[10] which show antiplasmodial activity against *Plasmodium falciparum*. Other examples are ervatensine A and B (**11** and **12**, fig. 4) from *T. corymbosa*, which showed growth inhibitor activity against lung, colon and breast cancer cell lines.^[11] Additionally, conophyllin (**13**), which was isolated from *T. divaricata*^[12], promotes insulin production in rat pancreatic cells.^[13]

Tabernaemontana donnell-smithii is native to Mexico and Central America and belongs to the family *Apocynaceae*, like the alkaloid producing species *T. sissilifolia*, *T. corymbosa* and *T. divaricata*. However, the alkaloid profile of this plant has not been well studied. Therefore, it is a good candidate for identification of new BIA natural products.

1.2 Biosynthesis of aspidosperma and iboga scaffolds

The biosynthesis of all MIAs starts from two building blocks: tryptophan (**14**) and the monoterpene iridoid secologanin (**15**). Tryptophan is decarboxylated to form tryptamine (**16**) (scheme 1).^[14] Tryptamine is then condensed with secologanin by strictosidine synthase in a Pictet-Spengler-like

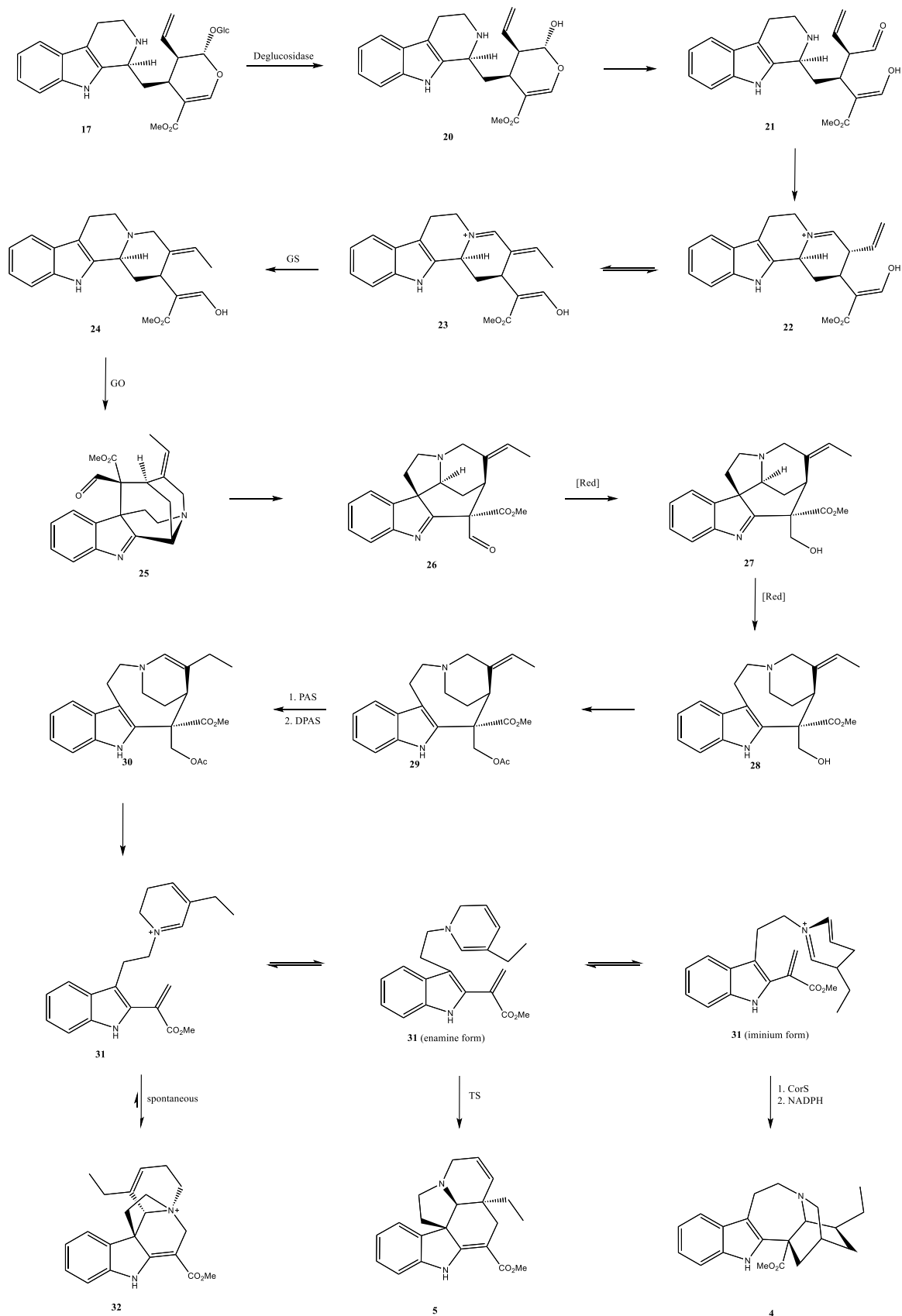
reaction to form strictosidine (**17**).^[15] Compound **17** is the central starting point for all MIAs, including **2**, **3**, ajmaline (**18**), camptothecin (**19**) and many more.



Scheme 1: Biosynthesis of strictosidine (**17**) from tryptophan (**14**) and secologanin (**15**) and follow-up products of **17**.

To proceed further, the hydrolysis of the glucose on strictosidine is catalysed by a β -glucosidase (scheme 2).^[16] The newly formed hemiacetal (**20**) degrades quickly to a dialdehyde intermediate (**21**). One of the aldehyde moieties in the molecule is now capable of condensing with the secondary amine in the tetrahydro- β -carboline unit of the molecule to form 4,12-dehydrocorynantheine aldehyde (**22**). **22** can isomerize to form 4,12-dehydrogeissoschizine (**23**), which is ultimately converted to preakkumanicine (**27**).^[15] New model studies and the isolation of two enzymes suggest, that **23** is first reduced by an alcohol dehydrogenase (GS) to geissoschizine (**24**), which then gets oxidized by GO to rhazimal (**25**).^[17] Rhazimal undergoes a rearrangement to form dehydropreakkumanicine (**26**) which gets reduced to form **27**. One more reduction step leads to stemmadenine (**28**). It was shown, that an acetylated version of **28**, stemmadenine acetate (**29**) is a competent precursor for the following biosynthetic steps.^[18] Next, an oxidation/reduction sequence, catalysed by PAS and DPAS respectively, leads to a net isomerisation of the double bond to yield dihydroprecondylocarpine acetate (**30**). Compound **30** is not stable and quickly degrades to dehydrosecodine (**31**), which is not stable either, but forms an intermediate called angryline (**32**).^[19] In the presence of either Tabersonine Synthase (TS) or Coronaridine Synthase (CorS), the enamine form of **31** gets converted to **5** and the iminium form to a coronaridine-precursor.^[19] To get **4**

one further reduction step is needed. The cyclisation by TS or CorS resembles a net-[4+2]-cycloaddition, but it was shown that this reaction follows a stepwise mechanism.^[20]



Scheme 2 (page before): Biosynthesis of **5** and **4** starting from **17**. Characterized enzymes are listed: β -glucosidase, GS = geissoschizine synthase, GO = geissoschizine oxidase, PAS = precondylocarpine acetate synthase, DPAS = dehydroprecondylocarpine synthase, TS = tabersonine synthase, CorS = coronaridine synthase.

1.3 Aim of this work

The project aims to characterise a BIA produced by *T. donnell-smithii* and to lay the groundwork for understanding the mechanism of its biosynthesis. In the project unit I performed an alkaloid extraction of *T. donnell-smithii* leaves and a preparative HPLC-fractionation of that extract. The mass of the major substance contained in the purest fraction is $m/z = 705.36$. A literature search showed that there are three BIAs known with that exact mass. One of them is angustilongine C (**33**)^[21], one is called 14,15-dehydrotetrastachyne (**34**)^[22] and the last one 14,15-dehydrotetrastachynine (**35**)^[23] (fig. 5).

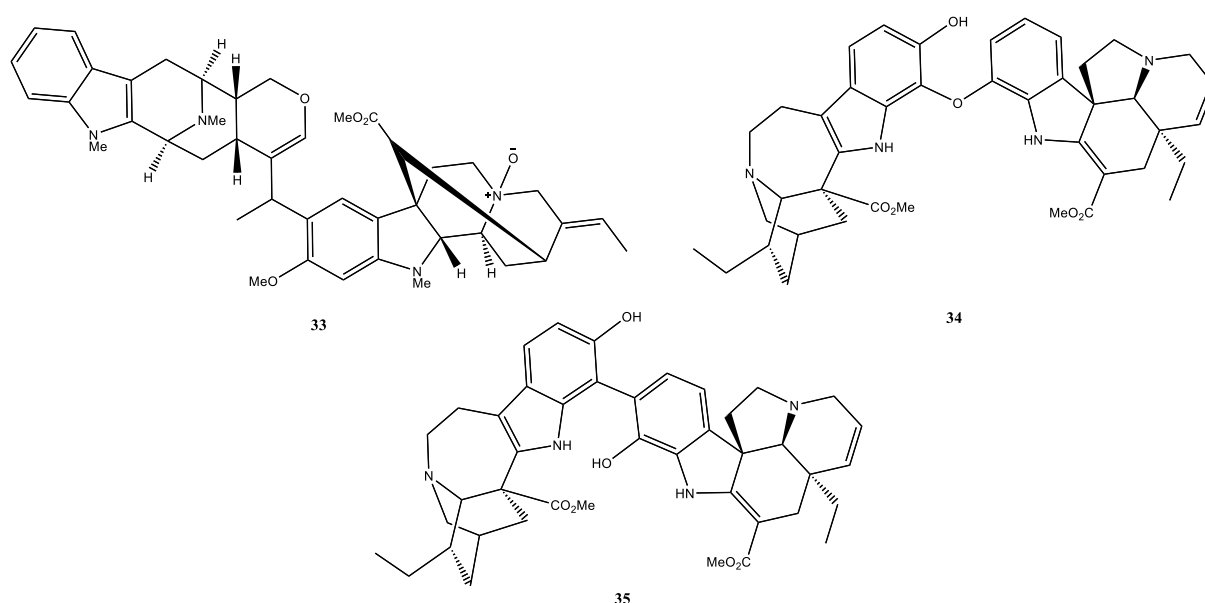


Fig. 5: Structures of angustilongine C (**33**) and 14,15-dehydrotetrastachyne (**34**) and 14,15-dehydrotetrastachynine (**35**)

In this thesis, I report the structural characterisation of the isolated compound by NMR-spectroscopy, and demonstrate that this compound is **34**. After the solving of the structure, experiments to understand how the dimerization to form this compound in the plant occurs.

Previously reported work used radioactively labelled **17** to demonstrate that this compound is a precursor for corynanthe, aspidosperma, and iboga type scaffolds in the plant *Catharanthus roseus*.^[24] I used a similar approach here, in which isotopically labelled **5** was fed to leaves of *T. donnell-smithii* to determine whether **5** was incorporated into the BIA. Due to the use of HR-MS stable isotopes can be used in place of radioactively labelled substances.

A second approach was the isolation of the enzyme(s) responsible for the dimerization. The structure of **34** suggests that an oxidation is involved in the dimerization. Oxidation reactions in plants are often catalyzed by P450 oxidases. Evidence can also be found in the biosynthesis of other biaryl ether natural

products, like vancomycin, which is performed by a series of P450 oxidases.^[25] Those enzymes are lipophilic and membrane bound,^[26] and therefore P450 enzymes are isolated by the preparation of the plant lipid fraction called microsomes.^[27, 28] Here I report the preparation of microsomes from different tissues of *T. donnell-smithii* and screened these microsomes with an *in vitro* essay for enzymatic dimerization activity.

2 Materials and Methods

2.1 NMR Analysis

In the project unit, 45.5 g of ground *T. donnell-smithii* leaves were extracted for half an hour using 500 mL of MeOH. After filtration the leave slurry was extracted again using the same method. The organic phases were combined and the MeOH was evaporated. After that the residue was dissolved in 270 of 0.012 M HCl and extracted six times with 100 mL EtOAc. The pH of the aqueous phase was adjusted to 10 using K₂CO₃ and was then extracted four times with 200 mL EtOAc. The combined organic phases were washed with brine. Evaporation of the solvent yielded 750 mg of a crude extract. This crude extract was filtered through a C18-SPE-column and was then subjected to preparative HPLC-fractionation. The purest fraction was used in this work and subjected to NMR analysis.

All of the previously obtained 7.5 mg in the purest fraction was dissolved in 2 mL H₂O. The pH was adjusted to 10 with K₂CO₃. The aqueous phase was extracted with 2 mL of CHCl₃. After evaporation of the solvent, the remaining solid was dissolved in 2 mL of water and freeze dried overnight. The solidified extract was dissolved in 600 µL of CDCl₃ and subjected to NMR Analysis on a 500 MHz Bruker ULTRASHIELD™ 500 Plus spectrometer.

2.2 Substrate feeding to *T. donnell-smithii*

A 70 mM solution of ¹³C-labelled tabersonine in MeOH was diluted to a 5 mM solution with PBS buffer (137 mM NaCl, 2.7 mM KCl, 10 mM Na₂HPO₃, 1.8 mM KH₂PO₄). This solution (1 mL) was infiltrated into a leaf of *T. donnell-smithii* using a plastic syringe. A second leaf was treated with 11.6 % MeOH in PBS buffer as a negative control. Both leaves were left on the plant for three days. After that time the leaves were harvested, frozen in liquid nitrogen and extracted with MeOH for 3 h. The MeOH extract was diluted and subjected to UHPLC-MS-analysis.

2.3 Root microsome preparation

Frozen plant material (5.35 g leaves, 6.61 g roots) of *T. donnell-smithii* was ground very finely in liquid nitrogen. The ground leaves were mixed with 20 mL of microsome-extraction-buffer (extraction buffer (50 mM Tris, pH 8.0, 2mM EDTA, 1 mM MgCl₂, 1 mM DTT) 1 g PVPP and 1 tablet of SIGMAFAST™ Protease Inhibitor Cocktail per 100 mL of buffer) and shaken for 0.5 h at 4 °C. After that the mixture was centrifuged at 72 g for 3 min, and the supernatant was collected. The remaining leaf slurry was treated with 20 mL of the extraction buffer and was shaken again for 0.5 h at 4 °C. The mixture was centrifuged again at 72 g for 3 min, the supernatant was collected and was combined with the first batch.

The mixed supernatants were centrifuged at 453 g for 5 min. The supernatant was then subjected to ultracentrifugation at 100,000 g for 1 h to pellet the microsomes. The supernatant was discarded and the remaining microsomes were suspended in 400 μ L of TEG buffer (50 mM Tris, pH 7.4, 1 mM EDTA, 20 % glycerol) and stored in 50 μ L aliquots, which were frozen in liquid nitrogen and stored at -80 °C.

2.4 Activity screening for microsomes

Microsomes were prepared from two plant organs: the Leaves (L) and the Roots (R). Their activity was tested using three substrates: tabersonine (Tab); labelled tab (13 C-Tab); and coronaridine (Cor). For each assay three samples were prepared: the first sample contained active microsomes (AM) and the two negative controls consisted of boiled microsomes (BM) or water (H_2O). So for example, the sample L-AM-Cor consists of active microsomes from the leaf and coronaridine as a substrate.

Since the purified microsomes carried metabolites from the plant two root samples were prepared to create a Metabolic Fingerprint (MF) from the active microsomes (AM) and the boiled microsomes (BM) to see, if there is a change in the endogenous metabolites occurring during the boiling process.

Microsomes were mixed with HEPES pH 7.5 buffer (50 mM, pH 7.5), NADPH (1 mM) and the substrates (coronaridine 80 μ M, tabersonine 40 μ M and 13 C-labelled tabersonine 40 μ M) were added separately (tab. 1). The vials were incubated for 24 h at 30 °C and were shaken at 800 rpm.

The same conditions were used for BM samples, except that the mixture of water and microsomes was boiled for 5 min at 80 °C and then kept on ice for 5 min prior addition of HEPES, NADPH and the substrate. Conditions for the water control were also the same, but instead of microsomes an equivalent volume of water was added.

After 24 h the reactions were quenched with 70 % MeOH (100 μ L). The samples were centrifuged at 21,130 g for 5 min to precipitate the membranes and the supernatant was analysed by UHPLC-MS.

To compare the metabolomic fingerprint between the boiled and non-boiled microsomes, 10 μ L of microsomes were mixed with HEPES pH 7.5 (50 mM) and extracted with MeOH 70%. The boiled sample was heated up to 80 °C for 5 min and after that kept on ice for 5 min prior to buffer addition and MeOH extraction. After centrifugation at 21,130 g for 5 min the samples were subjected to UHPLC-MS analysis.

All UHPLC-ESI-QTOF-MS analyses were done under the same conditions. Chromatography conditions: MeCN/ H_2O , 10:90 to 30:70, 8 min, 0.6 mL/min, Phenomenex Kinetex 2.6 μ m XB-C18 100 Å LC column 100x2.1 mm. For MS the positive mode was used

Tab. 1: volumes and final concentrations of each component in the microsome activity assay.

Sample	Microsomes (μL)	Substrate ($[\mu\text{M}]$)	HEPES pH 7.5 [mM]	NADPH [mM]
L-AM-Cor	10	Cor (80)	50	1
L-BM-Cor	10	Cor (80)	50	1
L-H ₂ O-Cor	0	Cor (80)	50	1
L-AM-Tab	10	Tab (40)	50	1
L-BM-Tab	10	Tab (40)	50	1
L-H ₂ O-Tab	0	Tab (40)	50	1
R-AM-Cor	10	Cor (80)	50	1
R-BM-Cor	10	Cor (80)	50	1
R-H ₂ O-Cor	0	Cor (80)	50	1
R-AM-Tab	10	Tab (40)	50	1
R-BM-Tab	10	Tab (40)	50	1
R-H ₂ O-Tab	0	Tab (40)	50	1
R-AM- ¹³ C-Tab	10	¹³ C-Tab (40)	50	1
R-BM- ¹³ C-Tab	10	¹³ C-Tab (40)	50	1
R-H ₂ O- ¹³ C-Tab	0	¹³ C-Tab (40)	50	1
R-AM-MF	10	0	50	-
R-BM-MF	10	0	50	-

3 Results

3.1 Structural characterisation of the isolated BIA of *T. donell-smithii*

In the ¹H-spectrum (fig A1) there are two vinylic protons with their characteristic shifts present (5.79 ppm and 5.72 ppm). Since they show COSY-correlations (fig. A5), the isolated compound cannot be **33**, because in this compound the two vinylic protons are in different parts of the molecule. Therefore **34** was used as a ground-scaffold for the structural elucidation.

For the structural characterization of the vinyl protons were chosen as a starting point due to their isolation in the ¹H-spectrum (fig A1). The carbon atom attached to each proton was determined via the HSQC-spectrum (fig A3). The exact shift of each carbon atoms was determined in the ¹³C-spectrum (fig. A2). This first assignment leads to the H-C pairs of 5.79 ppm - 125.1 ppm and 5.72 ppm - 133.3 ppm respectively (fig. 6).

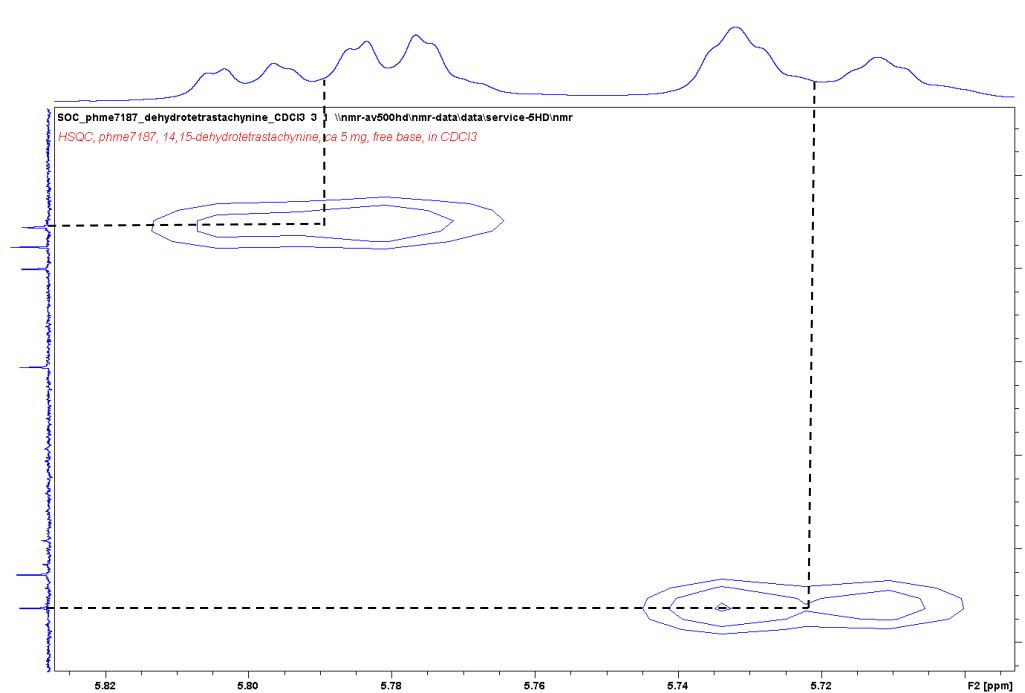


Fig 6: HSQC-correlations for vinylic positions

From that starting point, it was possible to identify carbon atoms linked via two and three bonds through the HMBC-spectrum (fig. A4). From the hydrogen atom with a shift of 5.79 ppm a correlation to two carbon atoms is visible with chemical shifts of 50.7 ppm and 41.5 ppm. The hydrogen atom with a shift of 5.72 ppm shows correlation to four carbon atoms with chemical shifts of 70.3 ppm, 50.7 ppm, 41.5 ppm and 27.3 ppm (fig. 7). Through HSQC correlations and the integrals taken from ^1H -spectrum it was possible to assign one quaternary carbon (C_q), one CH-group and two CH_2 group (δ : 70.3 ppm CH, 50.7 ppm CH_2 , 41.5 ppm C_q , 27.3 ppm CH_2).

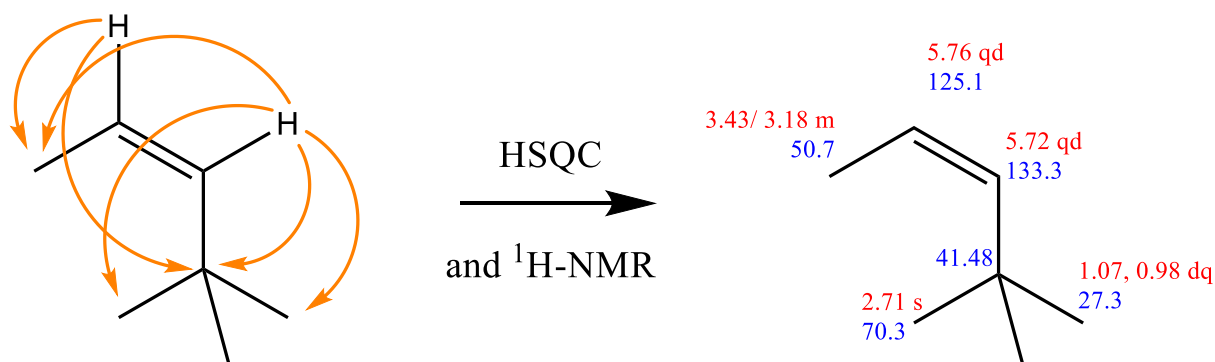


Fig 7: left: HMBC correlations (orange arrows) from the vinylic protons: right: chemical shift and multiplet of hydrogen (red) and carbon (blue) of the identified groups. For clarity's sake the coupling constants are not depicted

Using the methylene group with a shift of 1.07 and 0.98 ppm as a new starting point in the HMBC-spectrum, correlations can be observed to two new carbon atoms with chemical shifts of 28.9 ppm and 7.8 ppm (fig. 8). By HSQC-correlations, it is possible to identify them as a methylene and methyl group respectively. From the hydrogen with a chemical shift of 2.71 ppm HMBC-correlations show three new carbon atoms with shifts of 166.0 ppm, 140.7 ppm and 56.1 ppm. All of these carbons are quaternary positions.

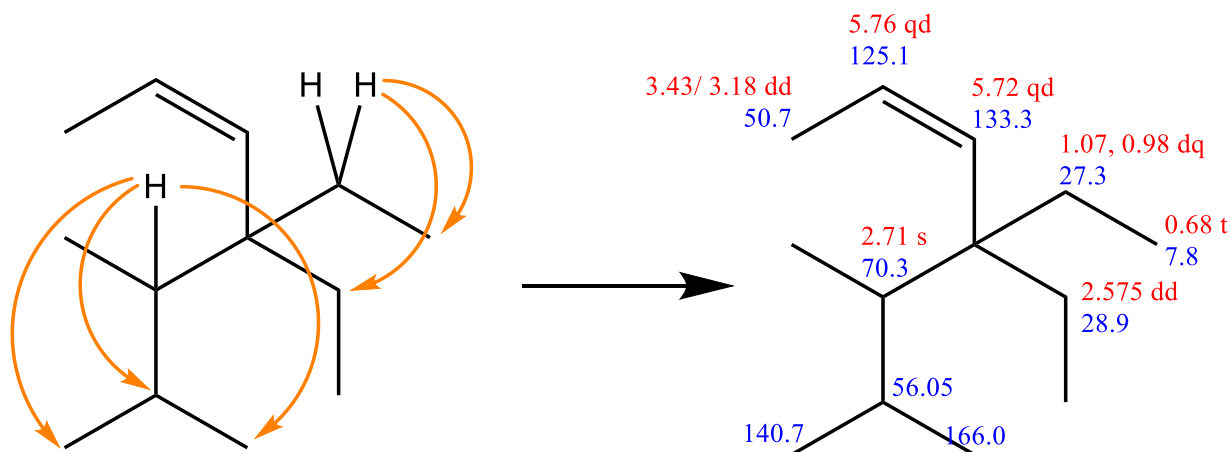


Fig 8: left: HMBC correlations (orange arrows) from the protons with a shift of 2.71 ppm and 1.07, 0.98 ppm, right: chemical shift and multiplet of hydrogen (red) and carbon (blue) of the identified groups. For clarity's sake the coupling constants and HMBC-correlations to already assigned groups are not depicted.

Using the newly identified methylene group as a starting point, three quaternary carbon atoms could be identified via HMBC-correlations (fig. 9). The chemical shifts of these carbon atoms are 169.0 ppm, 166.0 ppm and 93.8 ppm. Since the carbon atom at 166.0 ppm is already identified it is deduced that a six membered ring has to be present and since there is no other correlation except to the carbon at 169.0 ppm. It is deduced that the two carbons at 166.0 ppm and 93.8 ppm have to be connected by a double bond. Since a chemical shift of 169.0 ppm is characteristic of carbonyl groups, this center is assigned with such functionality

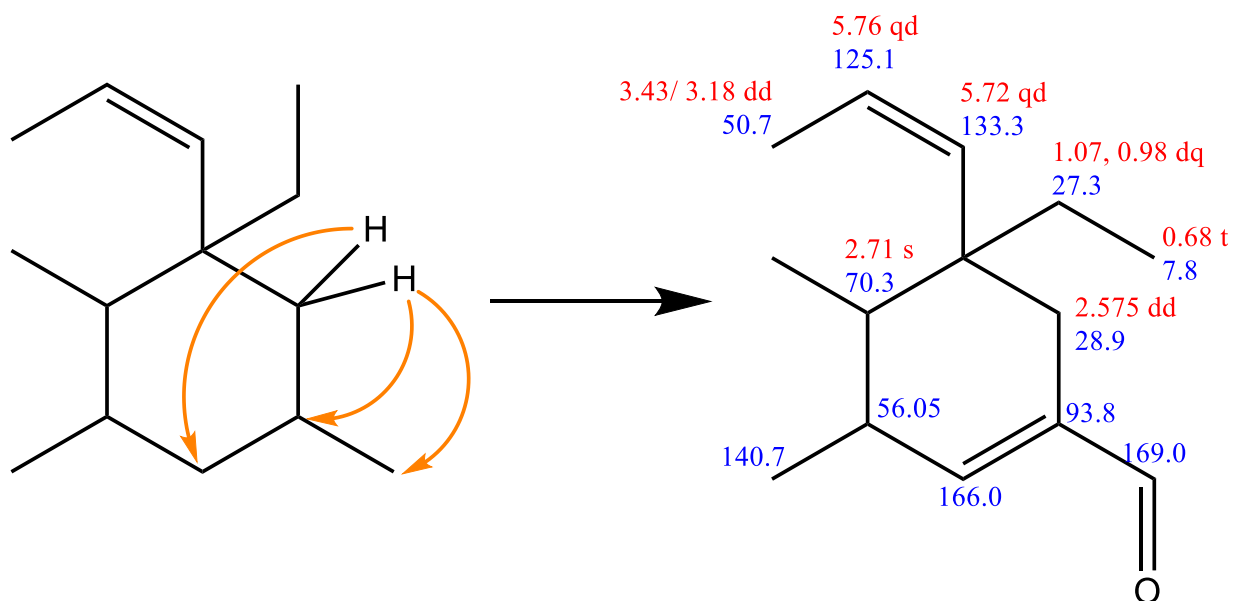


Fig 9: left: HMBC correlations (orange arrows) from the proton with a shift of 2.58 ppm; right: chemical shift and multiplet of hydrogen (red) and carbon (blue) of the identified groups. For clarity's sake the coupling constants and HMBC-correlations to already assigned groups are not depicted.

The newly assigned carbon atoms are used as starting points and hydrogen atoms that show correlation to these carbon atoms were then identified (fig. 10).

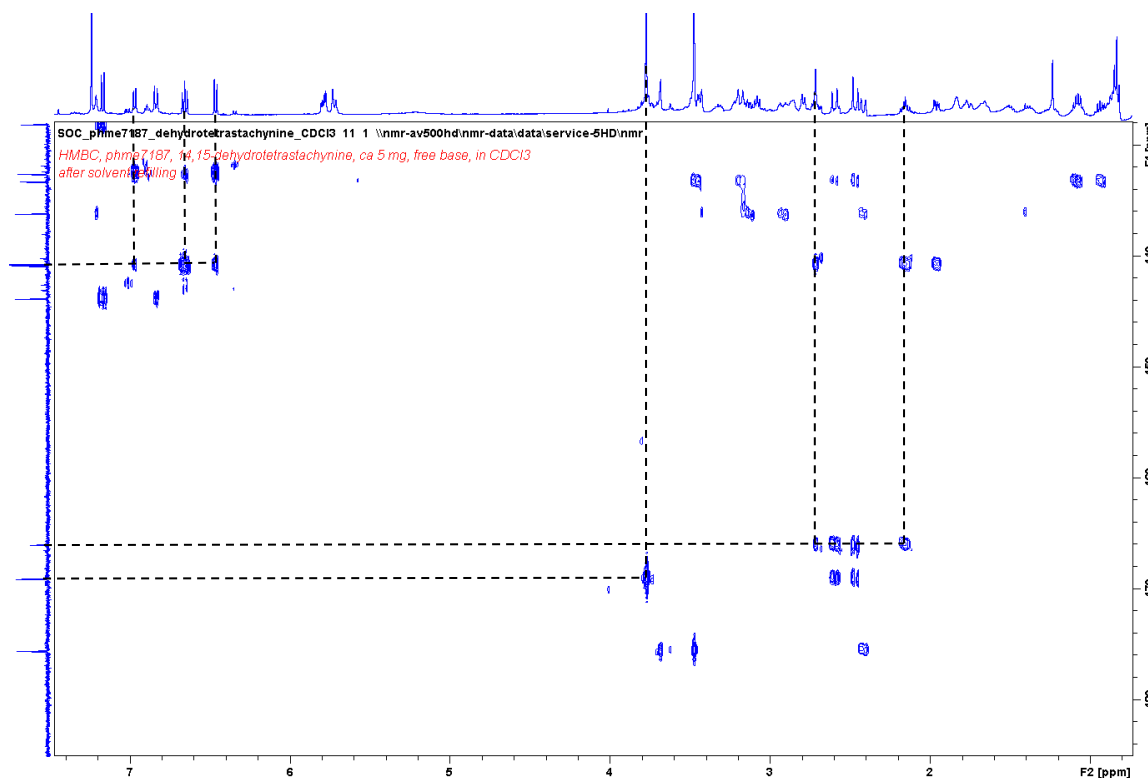
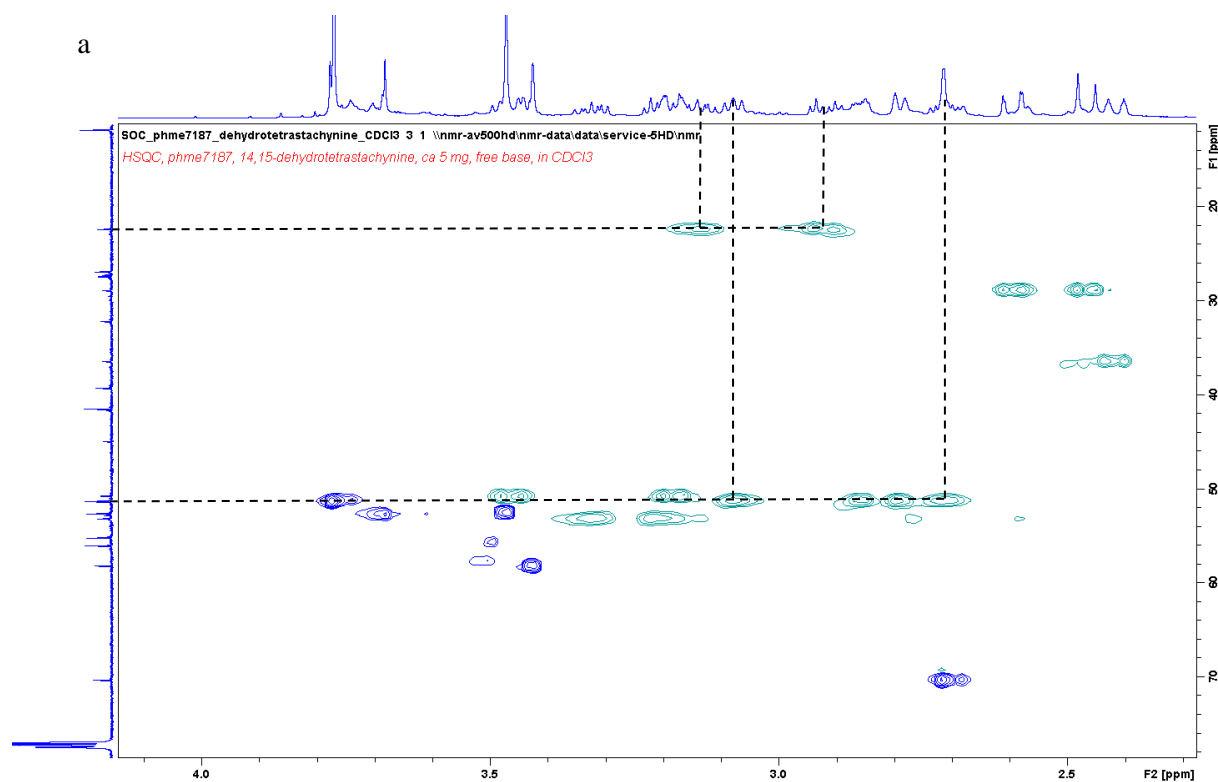


Fig. 10: HMBC correlations of the carbon atoms with chemical shifts of 169.0 ppm, 166.0 ppm and 140.7 ppm, for clarity's sake the previously found correlations are not depicted.

From the carbon at 169.0 ppm, a correlation is visible to a singlet hydrogen signal at 3.77 ppm (fig. 10), which is characteristic for methoxy groups. The carbon atom assigned to that group via HSQC with a chemical shift of 51.5 ppm and the integral in the ^1H -spectrum for that signal of three hydrogen atoms all indicate that this group is a methoxy group.

The carbon atom with a chemical shift of 166.0 ppm shows correlation to two new aliphatic hydrogen signals (fig. 11a). One with a chemical shift of 2.71 ppm and one with a shift of 2.15 ppm. An HSQC assignment of these signals reveals that there is one other hydrogen signal showing correlation to the same carbon atom for both groups individually (fig. 11b). The carbon atom with a chemical shift of 44.9 ppm correlates with CH_2 signals at 2.15 ppm and 1.95 ppm and the carbon atom at 51.2 ppm correlates with CH_2 signals 3.08 ppm and 2.71 ppm.



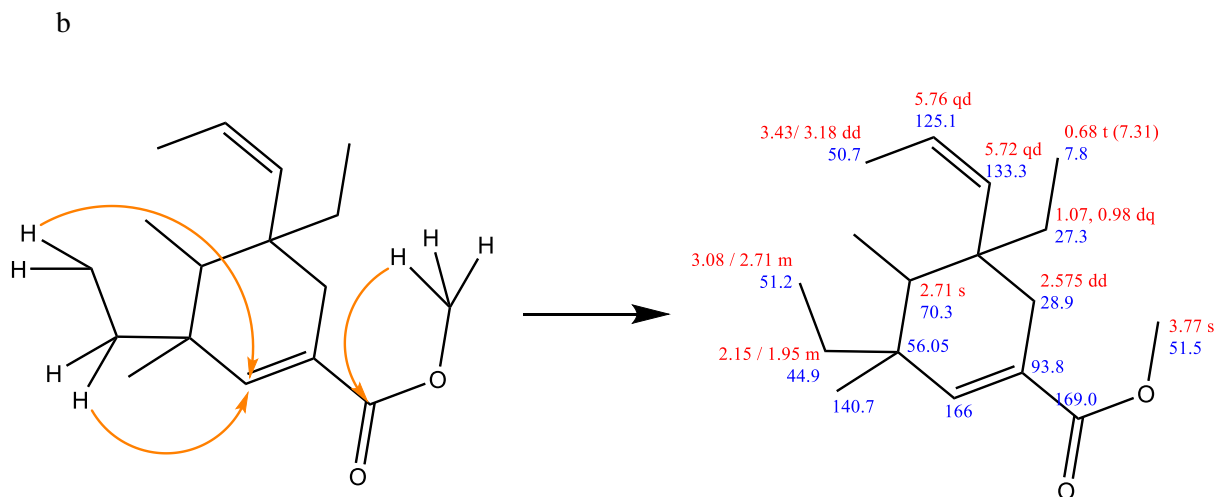


Fig. 11: a: HSQC correlations of the carbon atoms with chemical shifts of 51.2 ppm, 414.9 ppm and 140.7 ppm. b: left: HMBC correlations (orange arrows) from the proton with a shift of 2.15 ppm and from 2.71 ppm, right: chemical shifts and multiplets of hydrogen (red) and carbon (blue) of the identified groups. For clarity's sake the coupling constants and HMBC-correlations to already assigned groups are not depicted

From the carbon atom with a shift of 140.7 ppm, three aromatic hydrogen atoms are visible. The chemical shift of 140.7 ppm and the correlation to three aromatic hydrogen atoms indicate that this carbon atom is part of the aromatic system. The three visible correlations indicate that these three out of the five aromatic signals belong to this subunit of the bis-indole alkaloid. This can also be verified by the COSY-spectrum (fig. A5), where it is easily visible, that these three signals belong to one spin system, which means they are right next to each other. Since the hydrogen signal at 6.66 ppm (attached carbon signal at 121.5 ppm) shows correlation to the other two signals, this hydrogen is in the middle position between the hydrogens with a chemical shift of 6.97 ppm and 6.46 ppm with their attached carbon signals at 116.4 ppm and 114.2 ppm, respectively. The final assignment of this subgroup can be done via HMBC-correlations. Since the two hydrogen atoms at 6.97 ppm and 6.66 ppm show correlation to the quaternary carbon atom with a chemical shift of 56.1 ppm, those two groups have to be next to the carbon atom with a shift of 140.7 ppm. Through a combination of all the other HMBC-correlations from these three hydrogen atoms, all the other quaternary aromatic carbon atoms can be determined (fig. 12).

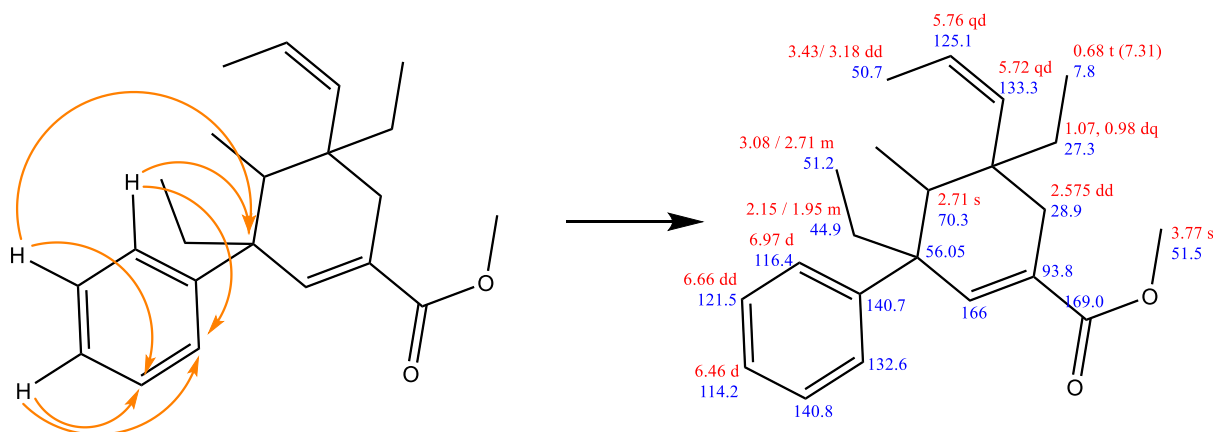


Fig 12: left: HMBC correlations (orange arrows) from the proton with a shift of 6.97 ppm, 6.66 ppm and 6.46 ppm, right: chemical shift and multiplet of hydrogen (red) and carbon (blue) of the identified groups. For clarity's sake the coupling constants and HMBC-correlations to already assigned groups are not depicted.

At this point the complete carbon skeleton is identified. The last step now is to determine the position of the two nitrogen atoms. The indole nitrogen contains one hydrogen atom. This hydrogen atom also shows a signal in the ^1H -spectrum and shows correlation two aromatic carbon atoms (fig. 13). The last open position, the aromatic quaternary carbon atom with a chemical shift of 140.8 ppm, which is assigned as an oxidized carbon atom, due to its high downfield shift, which is characteristic for such positions. The connection to the other part of the molecule probably happens over this oxygen atom, since there are no other HMBC-correlations in a new region visible. This subunit of BIA represents an aspidosperma scaffold, namely **5** which is oxidized at C-17.

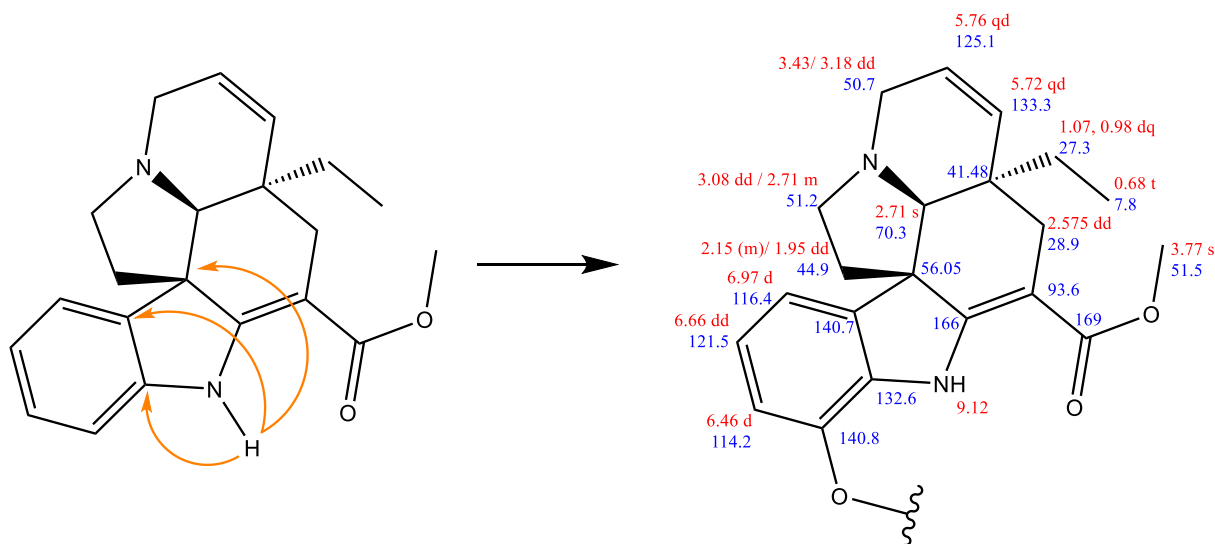


Fig 13: left: HMBC correlations (orange arrows) from the proton with a shift of the amine proton at 9.12 ppm, right: chemical shift and multiplet of hydrogen (red) and carbon (blue) of the identified groups. For clarity's sake the coupling constants are not depicted.

For the second monomer of the bisindole alkaloid, the second methyl group of the molecule, which is easily seen in the ^1H -spectrum is used as the starting point. Through HMBC-correlations two carbon

atoms could be identified (fig. 14). One with a chemical shift of 26.9 ppm, the other with a chemical shift 39.3 ppm. HSQC assignment leads to the identification of a methylene and one methyne group.

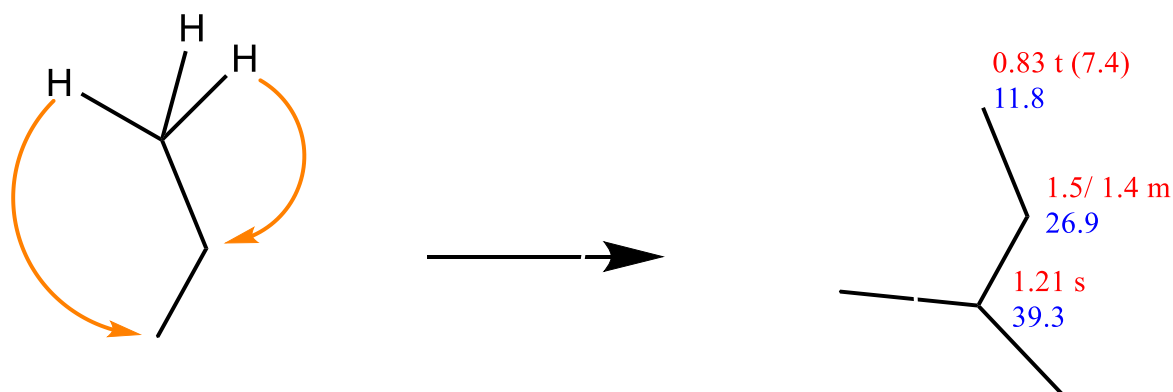
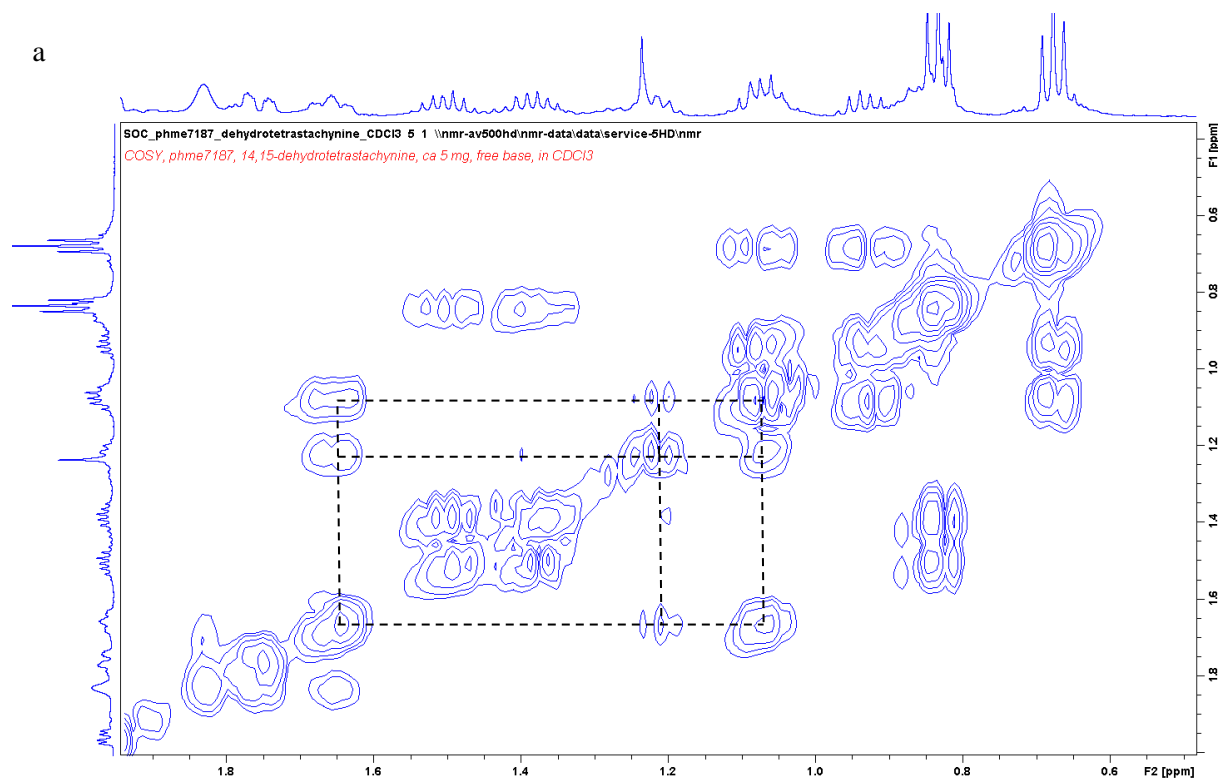


Fig 14: left: HMBC correlations (orange arrows) from the proton with a shift of 0.83 ppm, right: chemical shift and multiplet of hydrogen (red) and carbon (blue) of the identified groups. For clarity's sake the coupling constants are not depicted.

Further structural assignment is performed via correlations in the COSY-spectrum. From the hydrogen atom at 1.21 ppm, there is a COSY-correlation visible to a hydrogen atom at 1.64 ppm and 1.06 ppm (fig. 15a). An HSQC-assignment of these signals reveals that both hydrogen atoms (1.64 ppm and 1.06 ppm) belong to the same carbon atom (fig. 15b).



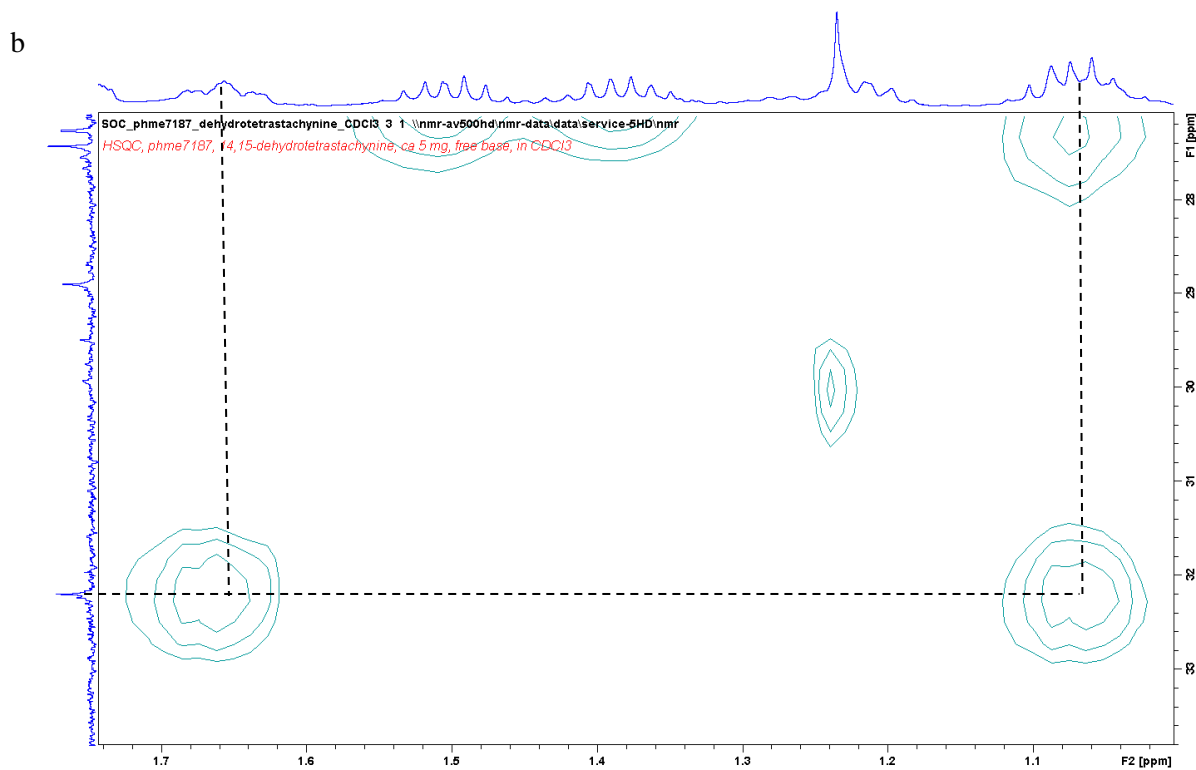
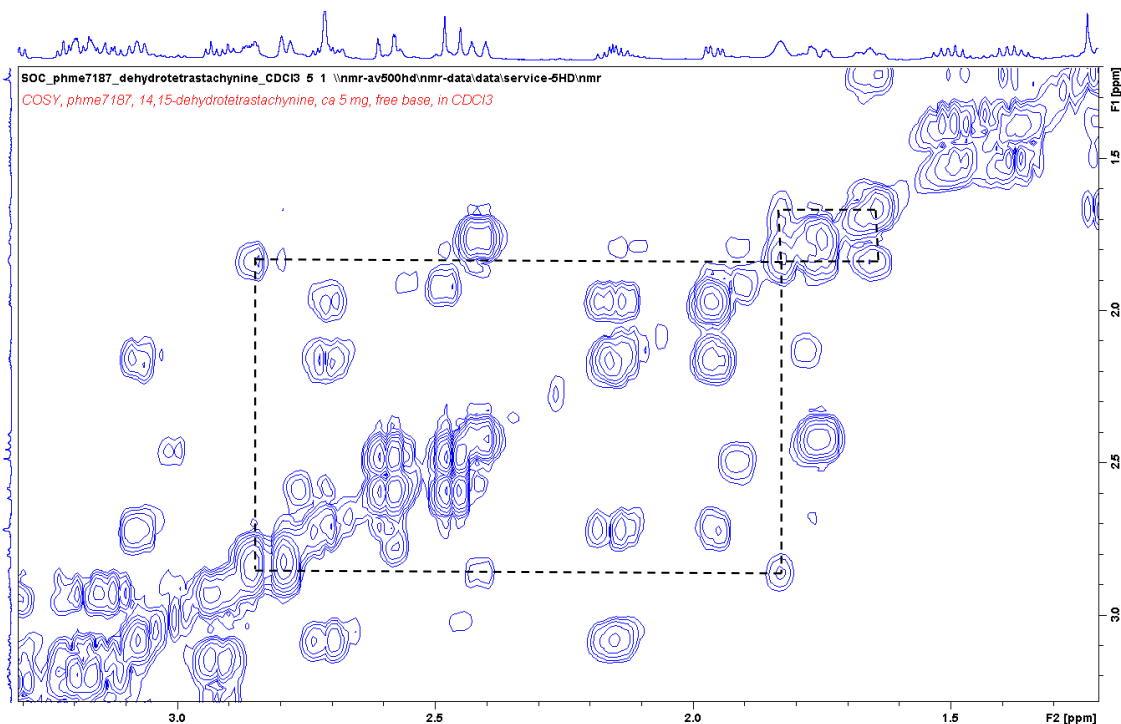


Fig. 15: a: COSY-correlations of the hydrogen atom with chemical shifts of 1.21 ppm, b: HSQC correlations for the hydrogen signals at 1.64 ppm and 1.06 ppm. For clarity's sake correlations to already identified signals are not depicted

Using the identified signal of 1.64 ppm as a new starting point in the COSY-spectrum, a correlation to a hydrogen signal at 1.83 ppm is visible and from that hydrogen signal, another correlation is detectable to a hydrogen signal at 2.86 ppm (fig. 16a). HSQC-assignment leads to the identification of a new methyne group and a methylene group (fig. 16b).

a



b

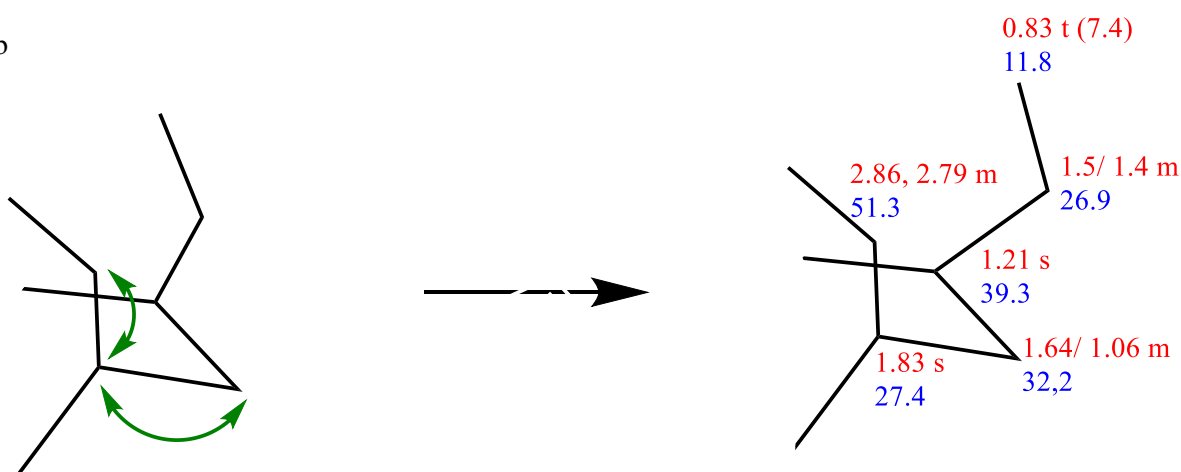


Fig. 16: a: COSY-correlations of the hydrogen atom with chemical shifts of 1.64 ppm and 1.83 ppm, b: COSY-correlations for the hydrogen signals at 1.64 ppm and 1.06 ppm (green arrows) and chemical shift and multiplet of hydrogen (red) and carbon (blue) of the identified groups. For clarity's sake correlations to already identified signals and coupling constants are not depicted.

Starting from the hydrogen signals at 2.86 ppm and 2.79 ppm, three new HMBC-correlations are visible (fig. 17a). Since there are no more visible COSY-correlations for these two signals, two of those three correlations must happen over a heteroatom, which is most likely to be a nitrogen. These three carbon atoms have a chemical shift of 58.3 ppm, 53.2 ppm and 36.4 ppm. The highest two shifts are in the range for carbon atoms next to a nitrogen atom. To identify if one of those two signals is in the already established spin-system, the TOCSY-spectrum (fig. A6) can be used. After HSQC assignment of these

three signals, it is clear that the carbon atoms with a shift of 53.2 ppm and 36.4 ppm (hydrogen shifts of 3.42 ppm and 2.41 ppm, 1.71 ppm respectively) are part of this spin system (fig. 17b), whereas the carbon atom at 58.2 ppm, with hydrogen signals at 3.32 ppm and 3.21 ppm, is not.

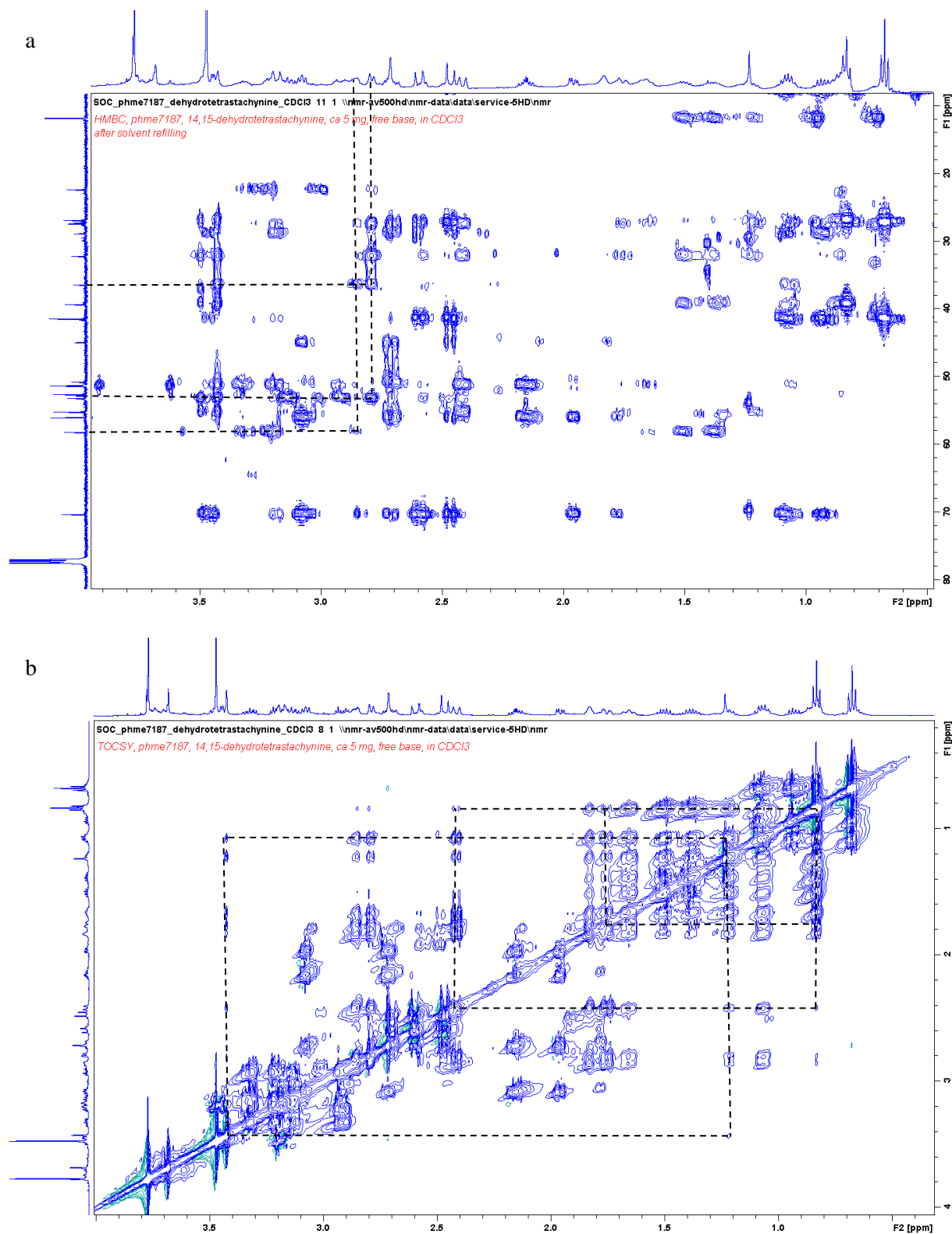


Fig. 17: a: HMBC-correlations of the hydrogen atoms with chemical shifts of 2.86 ppm and 2.79 ppm, b: TOCSY-correlations for the hydrogen signals at 3.42 ppm, 2.41 ppm and 1.75 ppm.

Collectively, this evidence leads to the identification of four new groups (fig. 18). Since there is also a HMBC-correlation between the hydrogen signal at 3.42 ppm and the carbon atom with a shift of 36.4 ppm, those groups have to be connected. Due to the fact, that the all TOCSY-signals of this spin-system are already assigned to a specific group, the connection must happen over a quaternary carbon atom. This quaternary carbon atom shows HMBC-correlations with the hydrogen signals at 2.41 ppm, 1.75 ppm and 1.21 ppm.

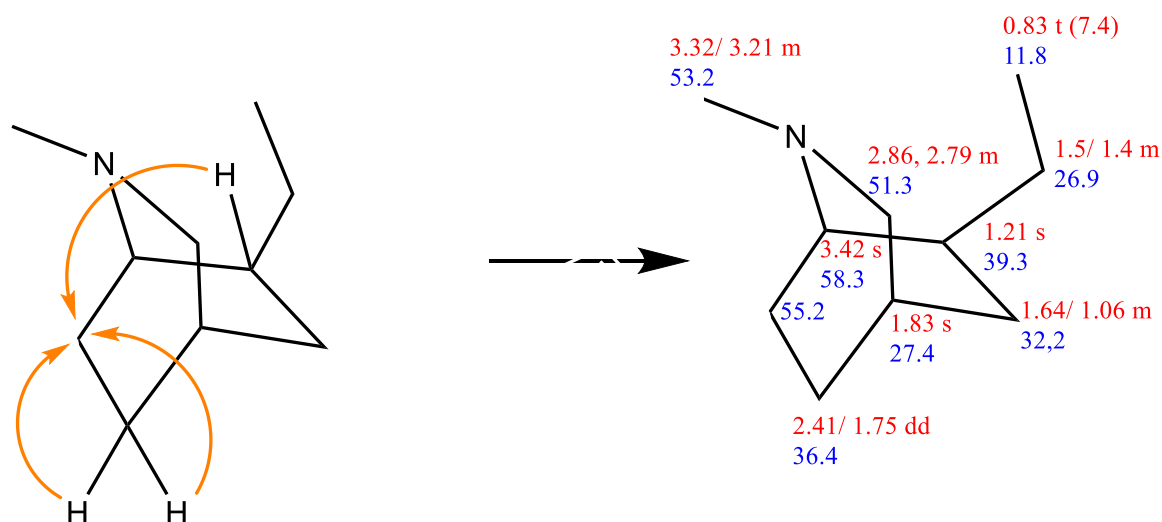


Fig 18: left: HMBC correlations (orange arrows) from the proton with a shift of 2.41 ppm, 1.75 ppm and 1.21 ppm, right: chemical shift and multiplet of hydrogen (red) and carbon (blue) of the identified groups. For clarity's sake the coupling constants and HMBC-correlations to already identified groups are not depicted

Using the newly assigned hydrogen signals at 3.32 ppm and 3.21 ppm as a starting point in the COSY-spectrum, there are two correlations visible at 3.13 and 2.92 ppm, which both belong to the same carbon atom at 22.4 ppm (fig. 19). HMBC correlations from these two hydrogen atoms reveal three new quaternary carbon signals at 136.0 ppm, 125.6 ppm and 111.0 ppm. Starting from the hydrogen atoms at 2.42 ppm and 1.75 ppm, there are two new HMBC-correlations visible. One to a quaternary carbon atom at 175.6 ppm and one to a carbon atom at 136.0. The last correlation indicates the presence of a seven membered ring. The signal at 175.6 could be assigned to a CO unit, due to its characteristic shift.

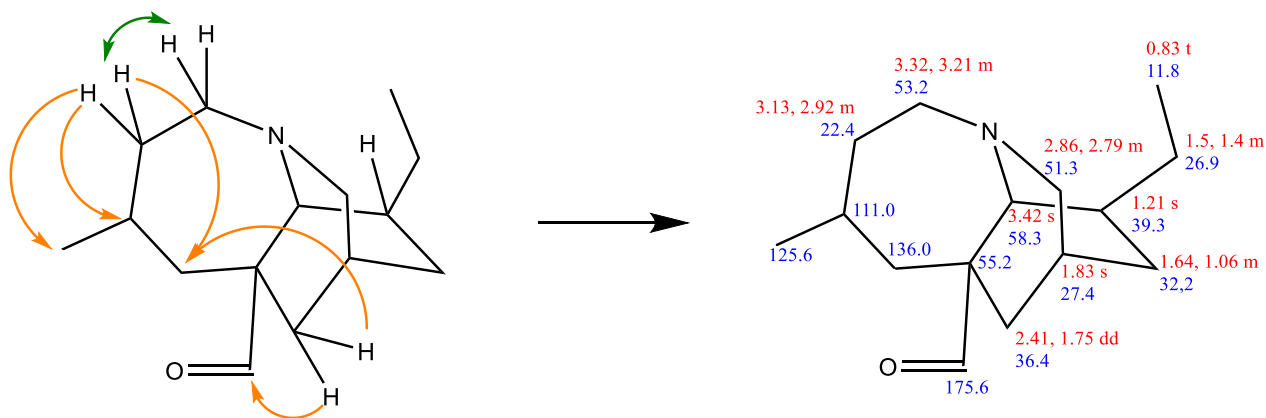


Fig 19: left: HMBC correlations (orange arrows) and COSY-correlation (green arrow) from the protons with shifts of 3.32 ppm, 2.41 ppm and 1.75 ppm, right: chemical shift and multiplet of hydrogen (red) and carbon (blue) of the identified groups. For clarity's sake the coupling constants and HMBC-correlations to already identified groups are not depicted

The carbon atom at 111.0 ppm shows HMBC correlation to the aromatic proton at 7.17 ppm (fig. 20). Taking into account that the remaining two aromatic hydrogen signals at 7.17 ppm and 6.84 ppm are doublets, with a coupling constant of 8.6 Hz and that they show COSY-correlation, it is possible to assume that they are next to each other.

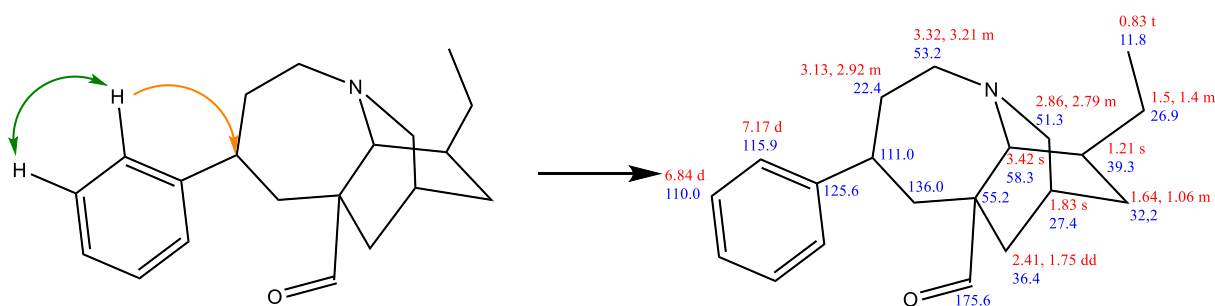


Fig 20: left: HMBC correlations (orange arrows) and COSY-correlation (green arrow) from the protons with shifts of 7.17 ppm and 6.84 ppm, right: chemical shift and multiplet of hydrogen (red) and carbon (blue) of the identified groups. For clarity's sake the coupling constants and HMBC-correlations to already identified groups are not depicted

The assignment of the remaining quaternary aromatic carbon atoms is done via HMBC-correlations from the two hydrogen atoms at 7.17 ppm and 6.84 ppm (fig. 21). In addition, it is searched for HMBC-correlations to the carbon atom at 175.6 ppm. Correlation to a proton singlet at 3.47 ppm indicates another methyl ester at this position. At this point the coronaridine skeleton for this monomer is completely assigned.

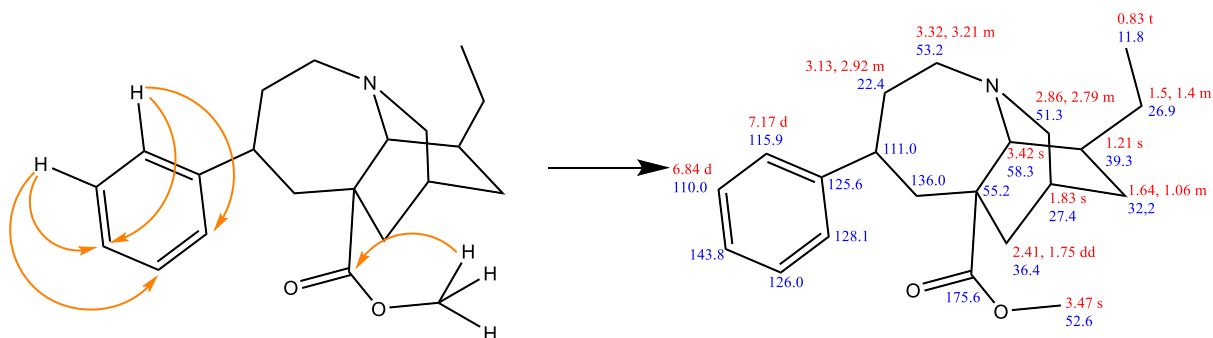


Fig 21: left: HMBC correlations (orange arrows) from the protons with shifts of 7.17 ppm and 6.84 ppm, right: chemical shift and multiplet of hydrogen (red) and carbon (blue) of the identified groups. For clarity's sake the coupling constants and HMBC-correlations to already identified groups are not depicted

Since the carbon skeleton is completely assigned the indole nitrogen has to be bound to the carbon atoms with the shifts of 128.1 ppm and 136.0 ppm. The hydrogen atom attached to the nitrogen atom has a chemical shift of 7.21 ppm and shows HMBC-correlations to the carbon atoms at 136.0 ppm, 125.6 ppm and 11.0 ppm. The carbon atom at 111.0 ppm and the one at 136.0 ppm are connected via a double bond.

At last the question remains, how both MIAs are connected. The two remaining quaternary aromatic positions are assigned as oxidized positions. Since there are no HMBC-correlations from the aspidosperma to the iboga subunit, the connection must happen via an oxygen atom and rules out **35**. A chemical shift of 143.8 ppm fits well to a free hydroxyl group attached to an aromatic system. A chemical shift of 126.0 ppm is quite unusual for an oxidized aromatic carbon, but if the oxygen at this position is functioning as an ether group, such a low chemical shift is normal. Therefore, the connection of the two structural subunits is happening over this oxygen atom as a biaryl ether (fig. 22).

After the connection of both subunits, the resulting BIA has an iboga-aspidosperma skeleton, represented by a hydroxylated coronaridine and a tabersonine subunit. After connection of the two MIAs the structure of **34** is verified

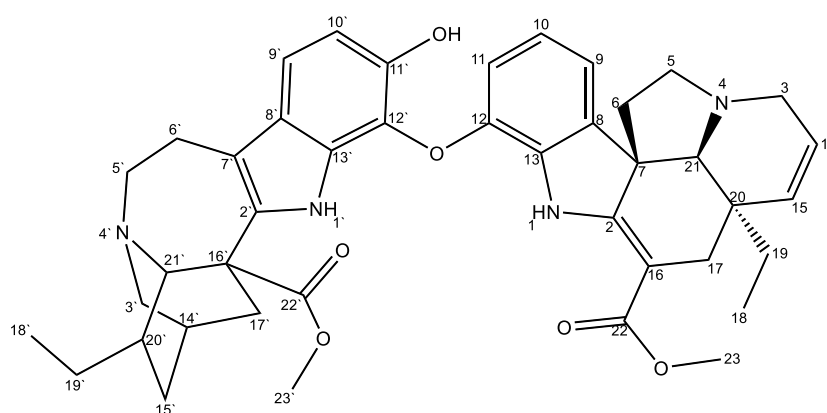


Fig. 22: Complete structure of isolated compound with annotations. Chemical shifts are presented in tab. 2

Tab. 2: Chemical shifts of the NMR-data from isolated compound.

Group number	¹ H-NMR Signal in ppm, multiplet (<i>J</i> in Hz)	¹³ C-NMR Signal in ppm	Group
1	9.12, s	-	NH
1'	7.21, s	-	NH
2	-	166.0	C _q
2'	-	136.0	C _q
3	3.48, 3.18. m	50.7	CH ₂
3'	2.86, 2.79 m	51.3	CH ₂
4	-	-	N
4'	-	-	N
5	3.08, 2.71, m	51.2	CH ₂
5'	3.32, 3.21 m	53.2	CH ₂
6	2.15 m, 1.95 dd (11.47, 4.70)	44.9	CH ₂
6'	3.13, 2.92 m	22.4	CH ₂
7	-	56.1	C _q
7'	-	111.0	C _q
8	-	140.7	C _q
8'	-	125.6	C _q
9	6.97 d (7.41)	116.4	CH
9'	7.17 d (9.09)	115.9	CH
10	6.66 dd (8.24, 7.41)	121.5	CH
10'	6.84 d (8.82)	110.0	CH
11	6.46 d (8.24)	114.2	CH
11'	-	143.8	C _q
12	-	140.8	C _q
12'	-	126.0	C _q
13	-	132.6	C _q
13'	-	128.1	C _q
14	5.79 dd (9.88, 4.62)	125.1	CH
14'	1.83 s	27.4	CH
15	5.72 d (9.95)	133.3	CH
15'	1.64, 1.06 m	32.2	CH ₂
16	-	93.6	C _q
16'	-	55.2	C _q

17	2.58 m	28.9	CH ₂
17 ^o	2.41, 1.75 m	36.4	CH ₂
18	0.68 t (7.32)	7.8	CH ₃
18 ^o	0.83 t (7.5)	11.8	CH ₃
19	1.07 q (7.53), 0.98 q (7.21)	27.3	CH ₂
19 ^o	1.5 td (14.04, 7.16) 1.4 td (14.10, 7.15)	26.9	CH ₂
20	-	41.5	C _q
20 ^o	1.21 s	39.3	CH
21	2.71 s	70.3	CH
21 ^o	3.42 s	58.3	CH
22	-	169.0	C _q
22 ^o	-	175.6	C _q
23	3.77 s	51.5	CH ₃
23 ^o	3.47 s	52.6	CH ₃

3.2 Substrate feeding to *T. donnell-smithii*

In this experiment ¹³C- labelled **5** was infiltrated into the leaf of *T. donnell-smithii*. The leaf was allowed to remain attached to the plant for 3 days, after which the metabolites were extracted and analysed by LC-MS. The mass of ¹³C- labelled **5** should be observed in the leaf metabolite extract at the same retention time as **5**. The mass of the ¹³C-tabersonine ($m/z = 339.35$ for $[M+H]^+$) (fig. 23) was visible, in the chromatogram, indicating that in the leaf treated with the ¹³C-tabersonine solution, the labelled substance is present in the leaf and not in the control. By comparison with non-isotopically labeled **5**, this peak can be assigned as tabersonine. ¹³C-tabersonine has a $t_R = 4.92$ min, $m/z = 339.19$

After establishing that ¹³C-tabersonine was taken up into the leaf tissue, the other compounds present in the metabolite extract were screened by mass-spectrometry to determine whether the ¹³C-tabersonine is incorporated into the BIAs. Therefore, the chromatograms of the ¹³C-tabersonine treated leaf and the control were compared (fig. 24).

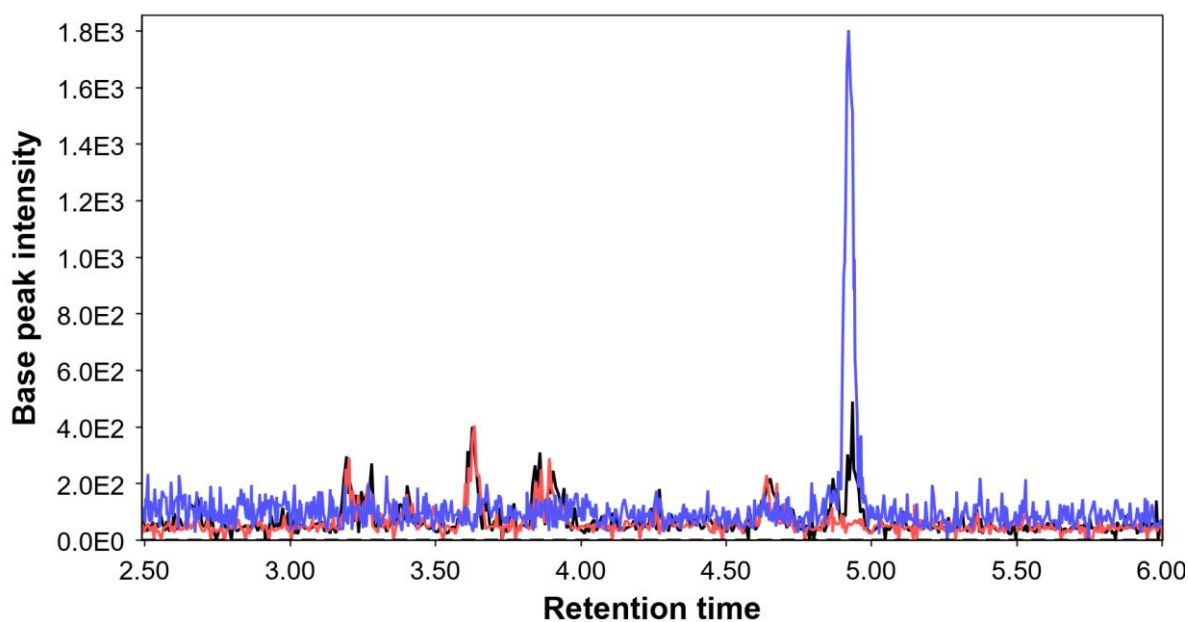


Fig. 23: chromatogram of the leaf treated with ^{13}C -tabersonine (black), the control leaf (red) and a tabersonine standard (blue), XIC: $m/z = 339.0000$ to 339.5000

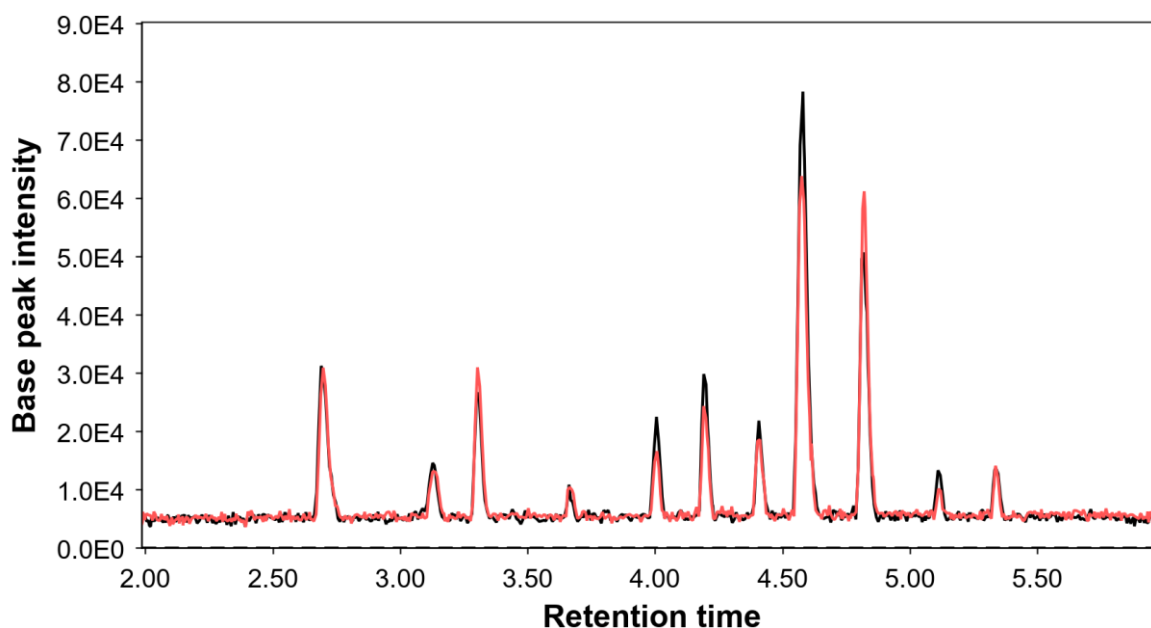


Fig. 24: chromatogram of the leaf treated with ^{13}C -labelled **5** (black), the control leaf (red), TIC

Since the masses of all compounds were the same, the intensities of the $[\text{M}+\text{H}]^+$ and the isotopic $[\text{M}+\text{H}+1]^+$ fragment were compared to see if there is any change in the isotopic distribution (tab. 3). For **34** at a $t_R = 5.33$ min there is no change in the isotopic distribution, as well as in most other peaks. However, a substantial change in the isotopic distribution for the compound at $t_R = 4.11$ min is detectable (fig. A7 and fig. A8). This compound is a BIA as well, since there is a $[\text{M}+2\text{H}]^{2+}$ fragment visible. Even though this substance has the same m/z as **34**, the structure of it is unknown.

Tab. 3: Peak list of all the BIAs of interest of the feeding experiment. For peak at 4.19 min, no [M+H] could be identified, for which it is not listed in this table.

t_R in min	m/z of [M+H] ⁺	¹³ C-tabersonine leaf			control		
		Intensity of [M+H] ⁺	Intensity of [M+H+1] ⁺	[M+H+1] ⁺ /[M+H] ⁺	Intensity of [M+H] ⁺	Intensity of [M+H+1] ⁺	Proportion of intensity
3.13	705.36	3.4 10 ²	2.3 10 ²	0.68	2.5 10 ²	1.8 10 ²	0.72
3.66	707.38	1.2 10 ²	1.1 10 ²	0.92	1.8 10 ²	1.3 10 ²	0.72
4.00	353.19	2.3 10 ⁴	5.2 10 ³	0.22	1.7 10 ⁴	4.3 10 ³	0.25
4.41	705.37	4.0 10 ²	2.9 10 ²	0.73	3.6 10 ²	1.3 10 ²	0.36
4.58	703.35	1.7 10 ³	7.9 10 ²	0.45	1.4 10 ³	5.8 10 ²	0.42
4.81	705.37	8.2 10 ²	3.0 10 ²	0.36	8.8 10 ²	4.8 10 ²	0.55
5.11	703.35	4.2 10 ²	1.6 10 ²	0.38	4.3 10 ²	1.3 10 ²	0.30
5.33	705.37	2.8 10 ²	1.6 10 ²	0.57	2.3 10 ²	1.4 10 ²	0.60

3.3 Microsome assay

Microsomes were isolated from *T. donnell-smithii* leaf tissue and used as a source of native *T. donnell-smithii* CYP enzymes. When microsomes were incubated with **5**, no conversion of **5** was visible as evidenced by LC-MS analysis (fig. 25a). The assays were screened for dimerization and mono oxidized products of **5** (fig. 25b), but no new products were observed. When **4** was used as substrate, the amount of substrate decreased during the assay (fig. 26a) in the sample with active microsomes (L-AM-Cor). However, this decrease is also visible in the L-BM-Cor sample, where the proteins should be denaturated and the intensity of all the other peaks in that sample is as high as in L-AM-Cor. Additionally, no new products were observed (fig. A9)

In the activity assay for microsomes isolated from root tissue (fig. 27), no reaction with **4** is observed, since the intensity of the peak of **4** does not decrease at all. However, **5** depleted after incubation with the microsomes (fig. 28). In all chromatograms, many peaks are present, which indicates, that there are many metabolites present in the microsomes.

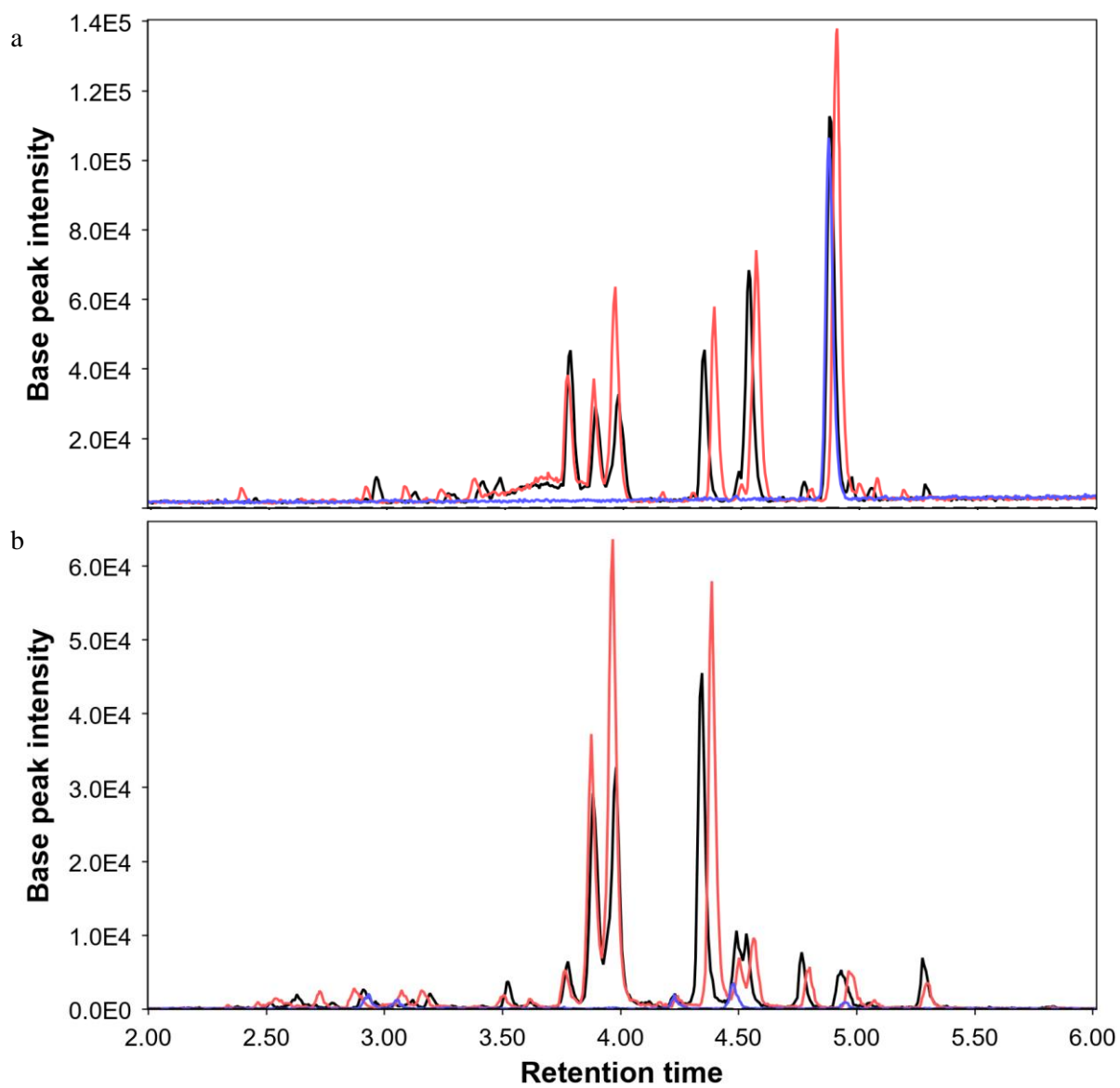


Fig. 25: Chromatogram of leaf microsome assay with **5**. a: TIC. b: XIC: $m/z = 353.0000$ to 353.5000 (monooxidized product). black: L-AM-Tab, red: L-BM-Tab, blue: L-H₂O-Tab

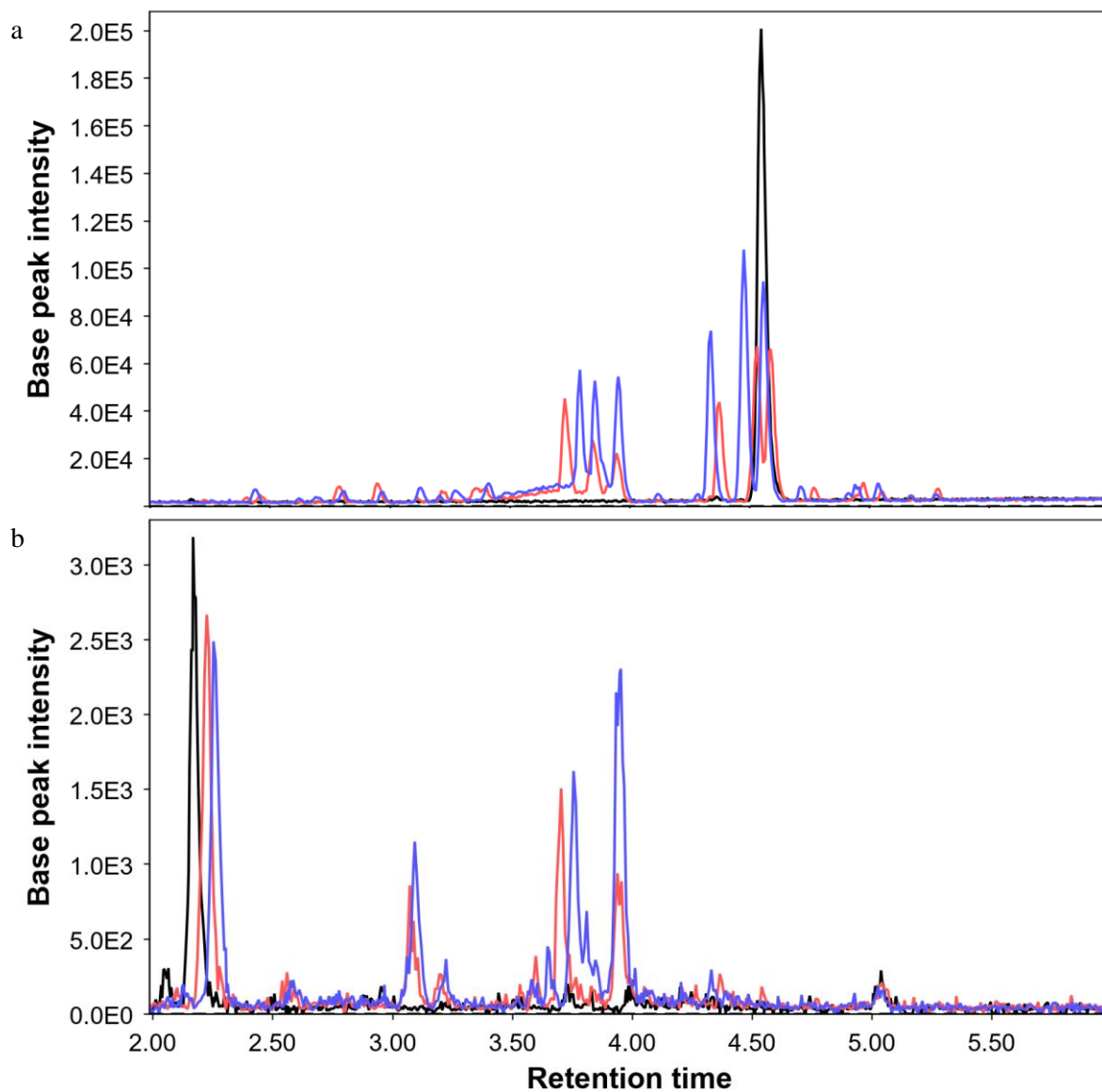


Fig. 26: a: Chromatogram of leaf microsome assay with **4**. a: TIC. B: XIC: $m/z = 355.0000$ to 355.5000 (monooxidized product), red: L-AM-Cor, blue: L-BM-Cor, black: L-H₂O-Cor

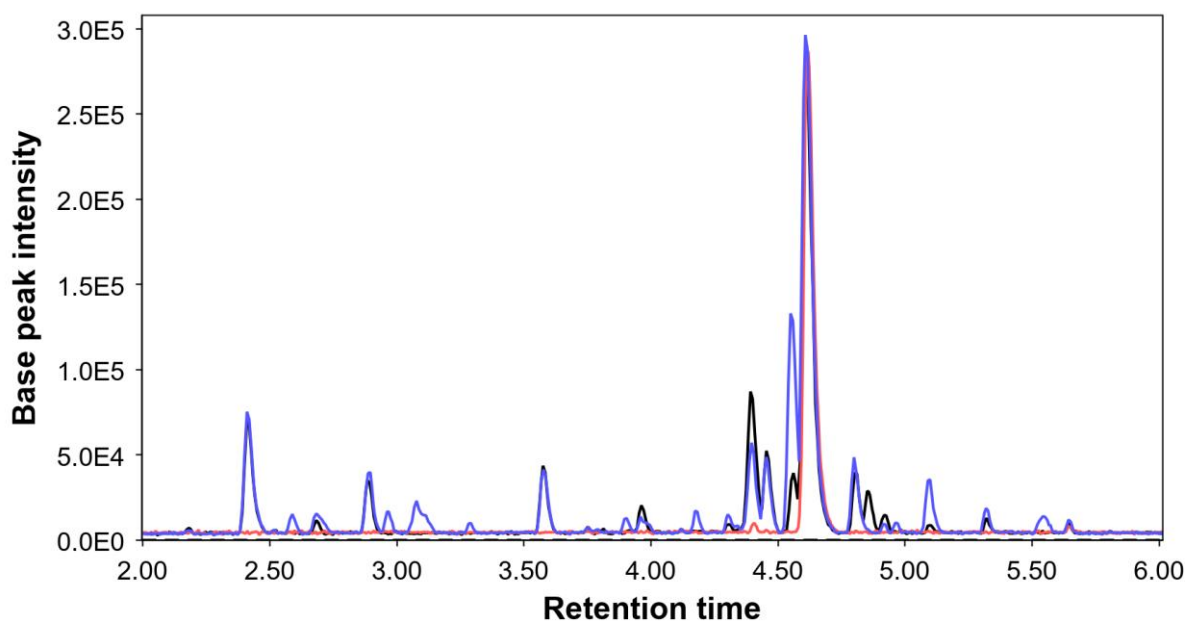


Fig. 27: chromatogram of root microsome assay with **4**, TIC, Black: R-AM-Cor, blue: R-BM-Cor, red: R-H₂O-Cor

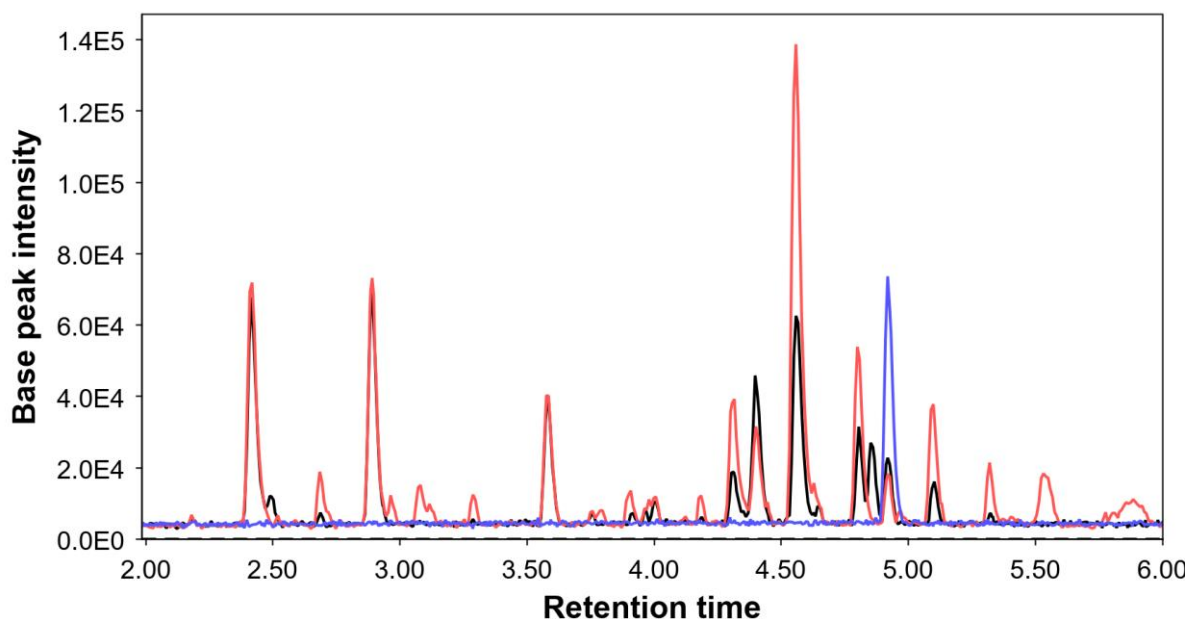


Fig. 28: chromatogram of root microsome assay with **5**, TIC, Black: R-AM-Tab, red: R-BM-Tab, blue: R-H₂O-Tab

To gain insight into what compounds are formed during the assay by the microsomes, ¹³C-labelled **5** was used as a substrate to trace a mass change in the formed products. In the chromatogram of the ¹³C-tabersonine assay (fig. 29) the same peak pattern is visible as in the assay in which **5** was used as substrate (fig. A10). The masses of specific peaks that are potential oxidation and dimerization products are compared in those two samples (tab. 4). Despite the consumption of ¹³C-tabersonine, there is no incorporation into the other compounds detectable.

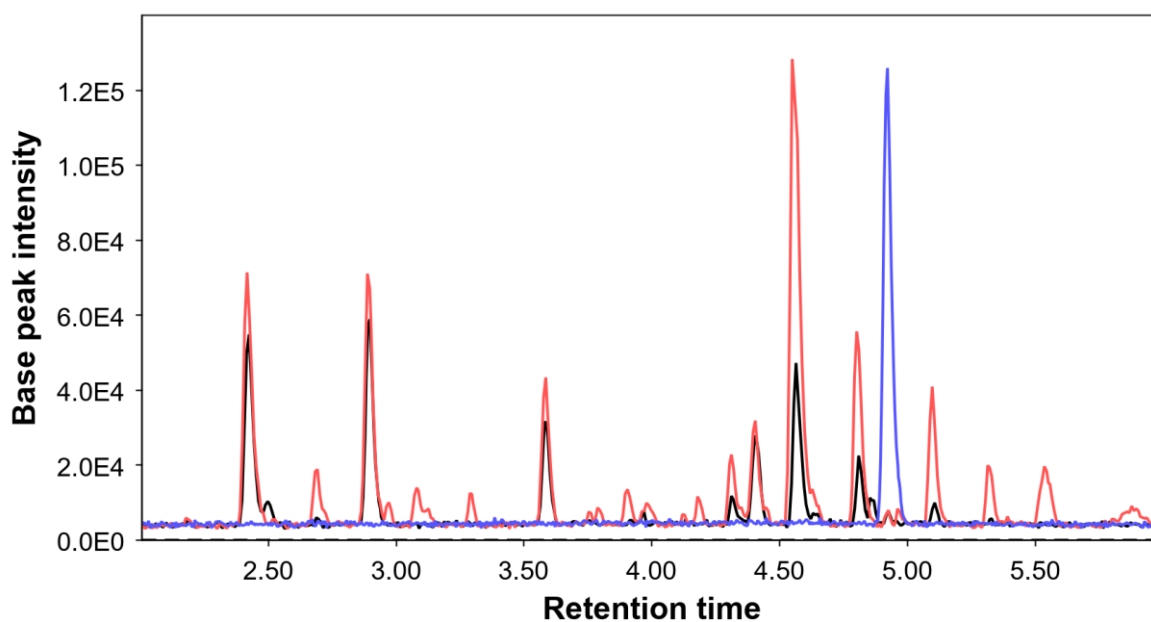


Fig. 29: chromatogram of root microsome assay with ^{13}C -labelled **5**, TIC, Black: R-AM- ^{13}C -Tab, blue: R-BM- ^{13}C -Tab red: R-H $_2$ O- ^{13}C -Tab

Tab. 4: m/z of $[\text{M}+\text{H}]^+$ of selected peaks from R-BM-Tab, R-BM- ^{13}C -Tab, R-AM- ^{13}C -Tab

T_R in min	m/z of $[\text{M}+\text{H}]$ in R-AM-Tab	m/z of $[\text{M}+\text{H}]$ in R-BM- ^{13}C -Tab	m/z of $[\text{M}+\text{H}]$ in R-AM- ^{13}C -Tab
2.96	355.20	355.20	-
3.07	353.19	353.19	-
3.30	353.19	353.19	-
3.91	705.36	705.37	-
4.18	352.17	352.18	-
4.31	353.19	353.19	353.19
4.40	353.19	353.18	353.18
4.56	703.35	703.35	703.35
4.81	705.36	705.36	705.36
4.86	353.19	-	-
4.92	337.19	337.19, 338.18	337.19, 338.18
5.10	703.35	703.35	703.35
5.32	705.37	705.37	705.37

To see what metabolites are present in the active microsomes and after the boiling process, the microsomes were extracted without the substrate. This confirms the presence of many metabolites (fig. 30) and especially the presence of a big amount of **5** ($t_R = 4.92$ and a m/z = 337.19). Also it is visible, that throughout the boiling process new substances are formed

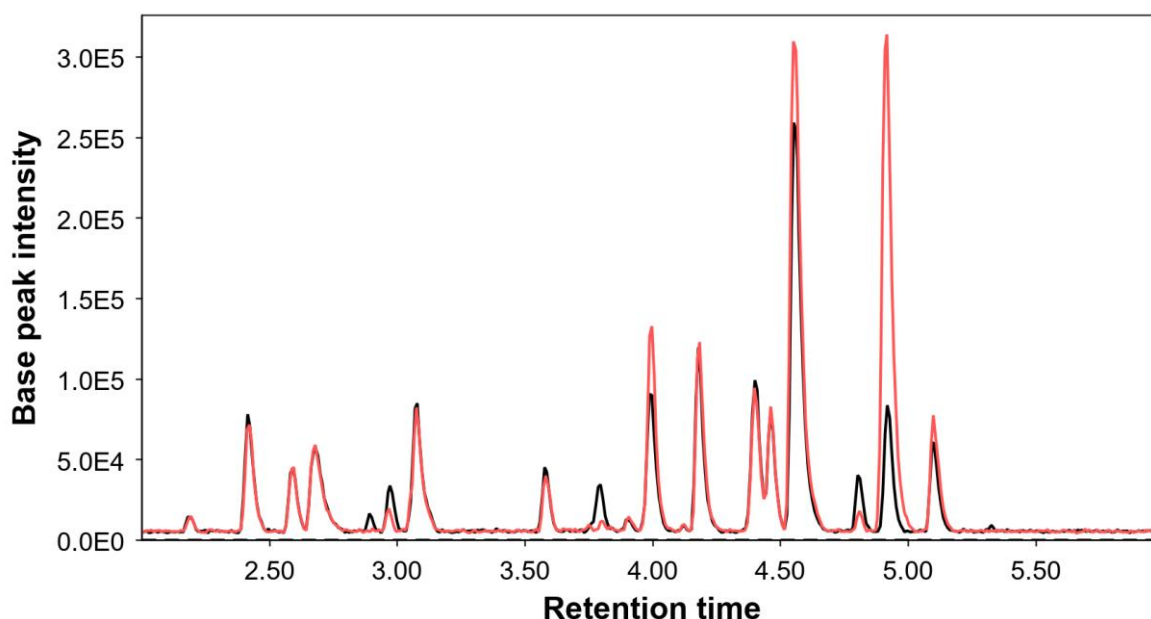


Fig. 30: chromatogram of metabolic fingerprint of the root microsomes. TIC. Black: R-AM, red: R-BM.

4 Discussion

4.1 Structural characterization of the isolated BIA of *T. donnell-smithii*

Through NMR-analysis it was possible to identify one of the major bis-indole alkaloids found in *T. donnell-smithii* leaves as **34**, a dimeric alkaloid in which hydroxylated **4** and **5** are linked via an ether bond. This compound was first isolated by Potier in 1984 from *T. citrifolia* and *T. siphilitica*^[22] It was not possible for them to assign every proton to a specific chemical shift, since there is a lot of overlap from the signals in the region of 2 ppm to 4 ppm. However, now the structure of **34** is fully elucidated and my work demonstrates that this substance is synthesized by *Tabernaemontana* species beyond *T. citrifolia* and *T. siphilitica*.

I did not assign the absolute stereochemistry of the monomer units. While the aspidosperma alkaloid exists in only one enantiomeric configuration in nature, both (+) and (-) iboga scaffolds are known. **4** always appears in nature as the (-) enantiomer, while catharanthine (**36**) exists as the (+) enantiomer. While it is most likely that the coronaridine monomer of this molecule is (-), we cannot definitively rule out that this monomer was derived from reduction of **36** (fig. 31). But since **4** and **5** are two natural products that are isolated from *T. donnell-smithii*,^[29] it is very likely that that **4** is part of the isolated BIA.

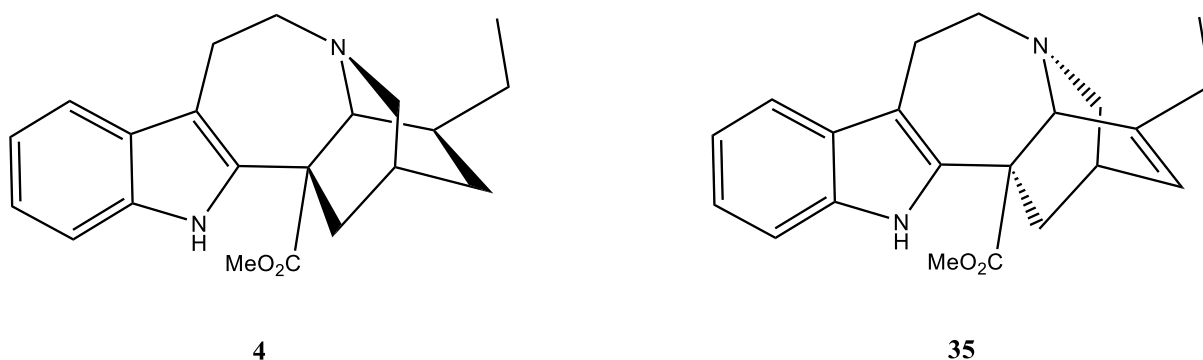


Fig. 31: Comparison of the structures of **4** and catharanthine (**36**)

4.2 Substrate feeding to *T. donnell-smithii*

With the structure of isolated **34** in hand, my research then turned to trying to understand how the dimerization of the coronaridine and tabersonine subunits happens. In feeding experiments with *T. donnell-smithii*, no incorporation of ^{13}C -tabersonine into **34** is detected. This negative result can be explained by many different reasons. The most obvious would be that the dimerization enzyme is not active in the leaf. Alternatively, it is possible that the ^{13}C -tabersonine was not taken up efficiently into the leaf, which is likely since the concentration of the labelled substance in the leaf extract is very low as evidenced by mass spectrometry (fig. 23). Nevertheless, it appears that ^{13}C -tabersonine is converted by the plant into at least one alkaloid, since there is a change in the isotopic pattern of one BIA visible at a t_R of 4.41 min. The identity of this BIA is not known, but the exact mass of 705.37 and the presence of a $[\text{M}+2\text{H}]^{2+}$ suggest that it is a BIA. It is not clear why ^{13}C -tabersonine is only incorporated into a single BIA, but it is possible that the biosynthetic enzymes for this BIA are most efficient (fastest) or expressed at the highest levels in this leaf tissue. Additionally, ^{13}C -tabersonine or derivatized products of ^{13}C -tabersonine could be distributed from the leaf throughout the plant; transport of alkaloids throughout diverse plant tissues is common.^[30]

4.3 Microsome assay

Since feeding studies led to inconclusive negative results, I isolated a membrane-protein fraction (microsomes) containing the plant P450 oxidases, enzymes that might be responsible for the coupling of the two subunits to form the dimeric compound. In the assay with the leaf microsomes with **5**, no conversion of **5** is visible. All substances in the chromatogram (fig. 24) can be found in the native (L-AM-Tab) and the boiled (L-BM-Tab) sample. Because this peak pattern is also visible in the assay with **4**, these substances are probably artefacts of the microsome preparation; it is likely that plant metabolites are present in this microsomal fraction. While the concentration of **4** decreases when incubated with microsomes, suggesting conversion by the enzymes present, the decrease is the same for the native sample L-AM-Cor and the boiled sample L-BM-Cor. This could be explained by the possibility, that **4** is diffusing into the microsomes due to its lipophilic nature. This would decrease the intensity of the substrate peak, but would not result in the increase or appearance of other peaks.

Since microsomes isolated from leaf did not appear to react with **4** or **5**, the roots were next chosen for microsome preparation and activity screening. In the root microsome assays, **4** is completely untouched by the microsomes. The intensity of the peak of **4** in all three samples (R-AM-Cor, R-BM-Cor, R-H₂O-Cor) is the same. However, there are even more peaks visible, than in the leaf-microsomes, suggesting that more metabolites are present in the root microsome preparations. The assay with **5** shows the same peak pattern for the native (R-AM-Tab) and boiled (R-BM-Tab) samples suggesting that no products are formed from **5**. However, the peak of **5** is completely consumed in R-BM-Tab.

To more effectively identify an enzymatic product, the assay was performed with ¹³C-labelled **5**. In this way, a mass shift in the substances that are created by the microsomes would differentiate them from the substances that are present from the extraction. Despite a complete conversion of labelled **5** (fig. 29), there is no mass shift visible for any compound (tab. 4). However, since the microsome preparations contain high concentrations of **5** (fig. 30), as further evidenced by a metabolome analysis of the roots that was done during the project unit (fig. A11), it is possible that only very low concentrations of labelled product were formed..

A metabolic fingerprint of the native and boiled microsomes was measured. The microsomes were extracted immediately after mixing with H₂O and HEPES 7.5 (R-AM) and right after the boiling process and mixing with HEPES 7.5 (R-BM). For R-AM many metabolites were visible and a strong peak at $t_R = 4.92$ min could be assigned as **5** (fig. 30). For R-BM the intensity of this peak gets smaller, which indicates that **5** gets converted during the boiling process. Probably over the course of heating up to 80 °C the enzymes get highly active, when the mixture is at around 40 °C. **5** is converted to the substances that are responsible for the peaks at a t_R of 2.89 min (352.18), 2.97 min (355.20), 3.80 min (395.20), 4.80 min (705.36) and 5.33 min (705.36), m/z in brackets. The peaks at 2.89 min, 4.80 min and 5.33 min represent BIAs, the compound at 5.33 is **34**. This is highly speculative, but it can be possible, that the proteins withhold these temperatures and are still active after the boiling process. This is indicated, that in the assay with labelled **5**, the peak of **5** completely vanishes for R-BM-¹³C-Tab.

Another fact that makes the interpretation of this assay quite difficult is the fact that the metabolic fingerprint of the microsomes is not consistent. For each assay, there are differences in the intensity of each peak and some different substances are produced (fig. A11). For R-BM-Tab and R-BM-¹³C-Tab another BIA at a t_R of 5.54 min is present. For these reasons, it is difficult to draw conclusions from assays with these microsome preparations. However, there is some evidence that the production of **34** happens in the roots, since it is not present in the metabolic fingerprint of the microsomes itself, but appears in some of the samples (R-BM-Tab, R-BM-¹³C-Tab and R-BM; fig. A12).

4.3 Outlook

The microsome preparation and assay needs to be further optimized. The extraction process needs to be modified so that metabolites are not present in this protein fraction. Since the use of organic solvents or

more acidic media is no option, because it would destroy the microsomes and enzymes in them, one way to purify them is to wash them with the TEG buffer more extensively or to purify them via dialysis before ultracentrifugation. The results of the assay would be more clear, if there are fewer background peaks in the chromatogram.

Additionally, isolation and identification of other BIAs in the plant presents some insights into the natural product scope of the plant. By identifying all the BIAs in *T. donnell-smithii*, a biosynthetic pattern could emerge, suggesting which monomers are used in the BIAs and how are they connected. If all the BIAs scaffolds are clear, it may be possible to hypothesize which enzymes are present in this plant, that are also present in other plants or some information about the promiscuity of the coupling enzyme(s) can be proposed. If more than just **4** and **5** are connected via an ether bond, it may be possible, that all these couplings are catalysed by one enzyme that accepts different substrates. In addition, transcriptomic data can be generated from the plant to then screen specifically for P450 oxidases and for homologs that catalyse the oxidative coupling. This would be more specific approach than just the extraction of all the lipophilic proteins from the plant.

After isolation of all the BIAs in *T. donnell-smithii* those samples can be used as standards to quantify their amount in different plant tissues to understand what substances are stored in which tissues. The quantification could also give some clues in what tissue what kind of coupling is happening, thereby specifying the search for the enzymes of interest.

Finally, the biological activity of **34** (and after isolation from the other BIAs) can be tested, to get insight into their potential use as drugs but also to gain some insight into the ecological role of those substances. For example, in this plant **5** is found at highest concentrations in the roots. Maybe **5**, or even BIAs are used as internal defence for plant pathogens, deterrents for herbivores or if they are even secreted into the soil to have an effect on bacteria and fungi present in the soil.

In general, there is much unknown about the biosynthesis of BIAs, making it an exciting prospect to understand the biosynthesis of such compounds. These studies could help make these compounds beneficial for humankind (e.g. as a treatment against a disease) and to understand the role of BIAs, and alkaloids in general, in the chemical network of nature.

5 Conclusion

Over the course of this work, it was possible to characterize *14,15*-dehydrotetrastachyne, with NMR-spectroscopy, as one of BIAs present in *T. donnell-smithii*. It was not possible to determine exactly the plant organ where the dimerization of the MIAs happens, since the data from the microsome assays (with enzymes from the leaf and roots) were too inconclusive. However, there is some evidence that the dimerization happens in the roots. This hypothesis still needs more investigation to be verified.

6 Zusammenfassung

Im Rahmen dieser Arbeit konnte 14,15-Dehydrotetrastachyne als eines der Bisindolalkaloide in *T. donnell-smithii* mittels NMR-Spektroskopie identifiziert werden. Es konnte jedoch nicht das Pflanzenorgan, in dem die Dimerisierung der Monoterpenindolalkaloide abläuft, bestimmt werden. Da die Daten der Microsomeassays (mit Enzymen aus dem Blatt und den Wurzeln) nicht sehr aufschlussreich sind. Allerdings gibt es Hinweise darauf, dass die Dimerisierung in den Wurzeln abläuft. Diese Hypothese bedarf noch mehr Forschung um verifiziert werden zu können.

7 Acknowledgement

I thank Sarah O'Connor that I was allowed to do my bachelor thesis in her lab. And I thank Dr. Thomas Wichard and jun.-Prof. Ivan Vilotijevic for making that possible. A big thank you goes to Dr. Francesco Trenti for supervising me over the course of this thesis and to Mohammed Omar Kamileen for giving me advice on how to prepare microsomes out of plant tissue and to Dr. Christian Paetz for giving me advice on how to solve complex structures via NMR-spectroscopy, as well as to the all the members of this group for giving me such a great time in the lab. I want to use this chance to thank Maximilian Meyer and Lucas Fritschka for their emotional support throughout the whole bachelors program. Without you I would not have come this far.

8 References

- [1] M. F. Roberts. M. Wink, **1998**, *Alkaloids – Biochemistry, Ecology and Medicinal Application*, 1st. Ed., Springer Science+Business Media, New York, 1 – 2
- [2] I. Jurna, *Schmerz*, **2003**, *17*, 280–283
- [3] Y. Remane, W. Reschetilowski, *Nachr. Chem.*, **2020**, *68*, 8-23
- [4] D. Weiß, *Chinin*, in F. Böckler, U. Dingerdissen, G. Eisenbrandt, *et al.*, RÖMPP [Online], **2020**, Georg Thieme Verlag, Stuttgart, available at: <https://roempp.thieme.de/lexicon/RD-03-01301>
- [5] R. Hänsel, **1994**, *Hagers Handbuch Der Pharmazeutischen Praxis*. Band 6: *Drogen P-Z.*, 5. Ed., Springer-Verlag, Berlin Heidelberg, 835–837
- [6] M. Kitajima, H. Takayama, **2016**, *Alkaloids: Chemistry and Biology*, *76*, 259-310
- [7] M. Moudi, R. Go, C. Y. S. Yien, M. Nazre, *Int J Prev Med.*, **2013**; *4*, 1231–1235
- [8] L. G. Wang, X. M. Liu, W. Kreis, D. R. Budman, *Cancer Chemother Pharmacol*, **1999**, *44*, 355–361
- [9] A Vacca, M. Iurlaro, D. Ribatti, M. Minischetti, B. Nico, R. Ria, A. Pellegrino, F. Dammacco, *Blood.*, **1999**,*94*, 4143-4155

- [10] M. Girardota, C. Deregnaucourta, A. Devillea, L. Dubosta, R. Joyeaua, L. Allorgeb, P. Rasoanaivoc, L. Mambu, *Phytochemistry*, **2012**, *73*, 65 – 73
- [11] K.-H. Lim, V. J. Raja, T. D. Bradshaw, *et al*, *Nat. Prod.*, **2015**, *78*, 1129–1138
- [12] T.-S. Kam, K.-Y. Loh, C. Wei, *Nat. Prod.*, **1993**, *56*, 1865-1871
- [13] K. Umezawaa, A. Hirokia, M.Kawakamia, *et al*, *Biomed Pharmacother*, **2003**, *57*, 341–350
- [14] P. J Facchini, K. L. Huber-Allanach L. W. Tari, *Phytochemistry*, **2000**, *54*, 121-138
- [15] S. E. O'Connor, J. J. Maresh, *Nat. Prod. Rep.*, **2006**, *23*, 532-547
- [16] I. Gerasimenko, Y. Sheludko, X. Ma, J. Stockigt, *Eur. J. Biochem.*, **2002**, *269*, 2204–2213
- [17] E. C. Tatsis, I. Carqueijeiro, T. Dugé de Bernonville, *et al.*, *Nat Commun*, **2017**, *8*
- [18] L. Caputi, J. Franke, S. C. Farrow *et al.*, *Science*, **2018**, *360*, 1235-1239
- [19] S. C. Farrow, M. O. Kamileen, L. Caputi *et al.*, *J. Am. Chem. Soc.*, **2019**, *141*, 12979–12983
- [20] L. Caputi, J. Franke, K. Bussey, *et al.*, *Nat. Chem. Bio.*, **2020**, *16*, 383-386
- [21] J. Soon-Yee, S. Navanesan, K.-S. Sim, *et al.*, *J. Nat. Prod.*, **2018**, *81*, 1266-1277
- [22] J. Abaul, P. Bourgeois, E. Philogene *et al*, *C. R. Acad. Sci., Ser.2*, **1984**, *298*, 627-629
- [23] J. Abaul, É. Philogéne, P. Bourgeois, *et al. J. Nat. Prod.*, **1989**, *52*, 1279-1283
- [24] N. Nagakura, M. Rüffer, M. H. Zenk, *J. Chem. Soc., Perkin Trans. 1*, **1979**, 2308-2312
- [25] R. D. Süssmut, W. Wohlleben, *Appl Microbiol Biotechnol*, **2004**, *63*, 344–350
- [26] B. Meunier, S. P. de Visser, S. Shaik, *Chem. Rev.* **2004**, *104*, 3947–3980
- [27] P. R. Rich, D. S. Bendall, *Eur. J. Biochem.*, **1975**, *55*, 333-341
- [28] C. Grand, *FEBS Lett.*, **1984**, *169*, 7-11
- [29] O. Collera, F. Walls, A. Sandoval, F. Garcia, J. Herran, M. C. Perezamador, *Boletin del Instituto de Quimica de la Universidad Nacional Autonoma de Mexico*, **1962**, *14*, 3-18
- [30] K. Yazaki, *FEBS Lett.*, **2006**, *580*, 1183-1191

Appendix

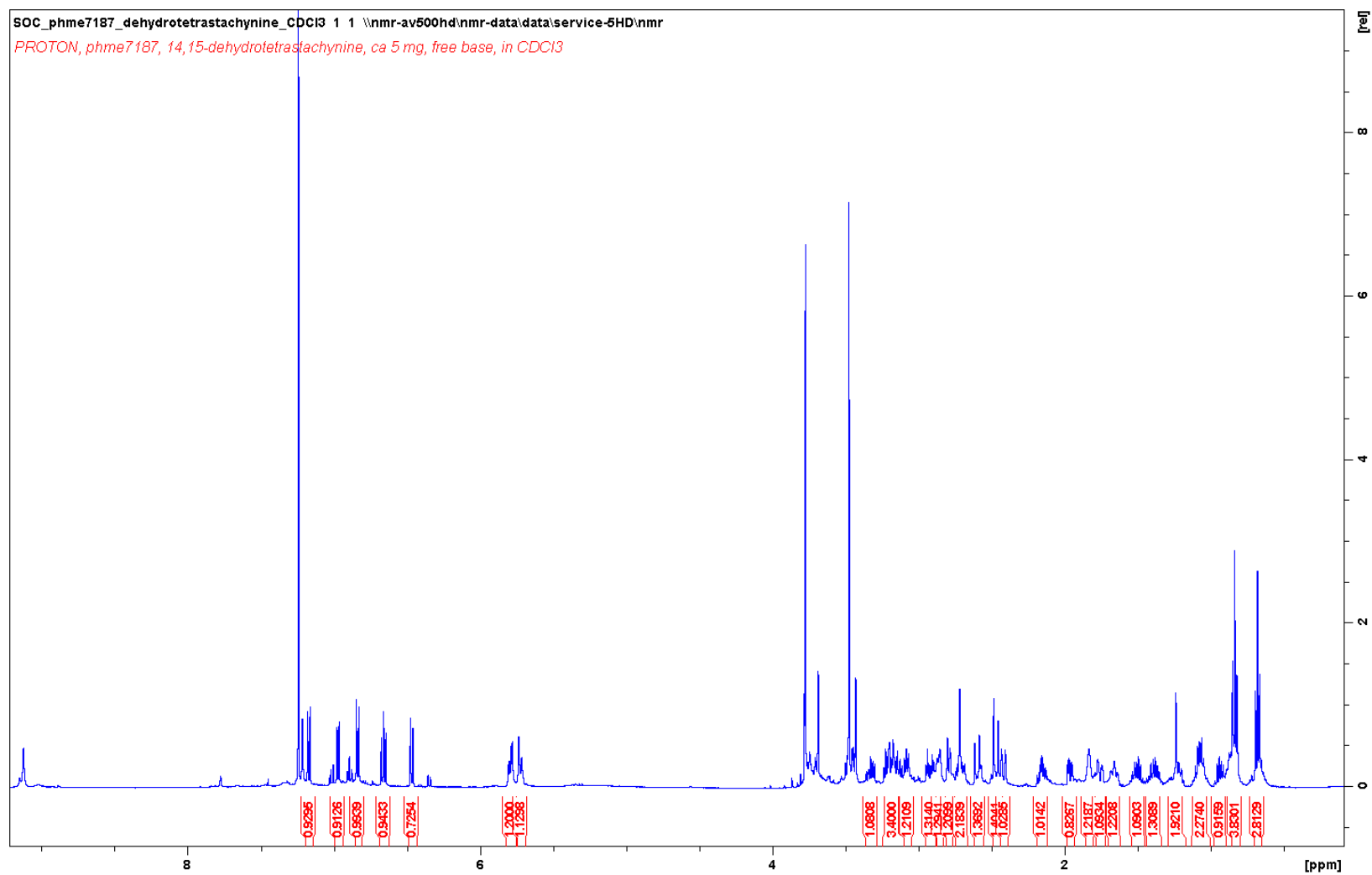


Fig. A1: ¹H-NMR spectrum **34** in CDCl₃, 500 MHz

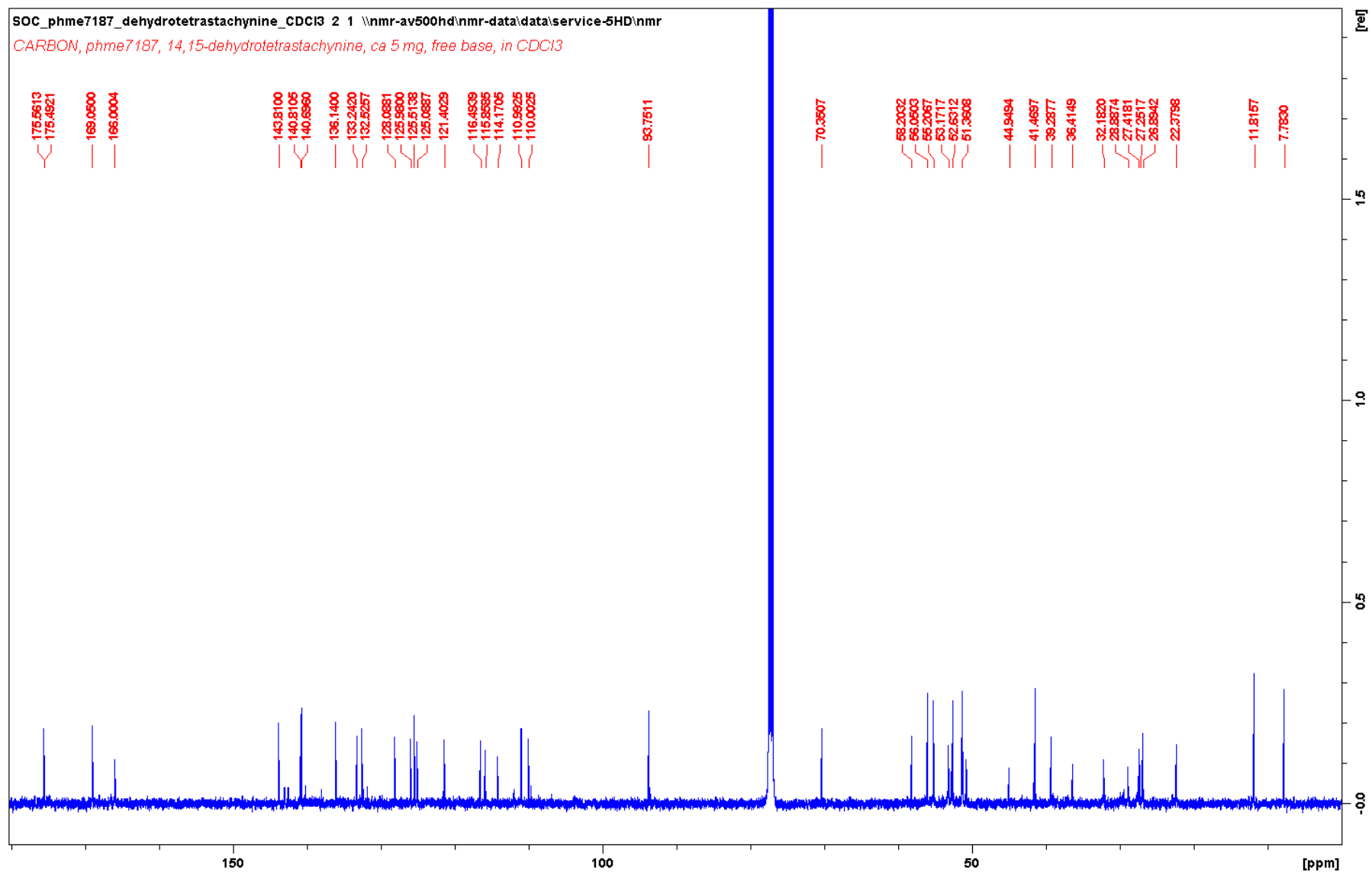


Fig. A2: ^{13}C -NMR spectrum of **34** in CDCl_3 , 500 MHz

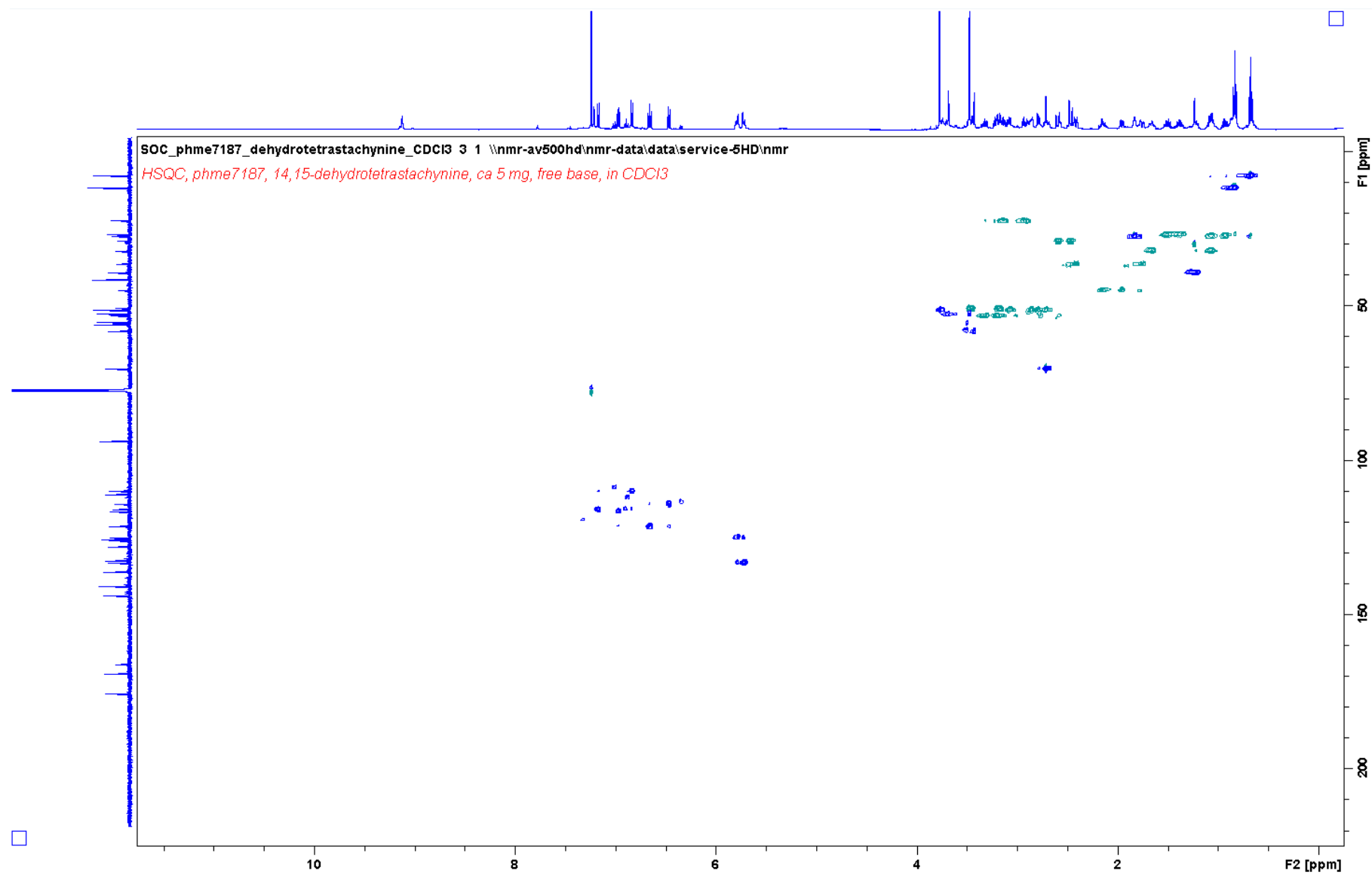


Fig. A3: HSQC-NMR spectrum of **34** in CDCl₃, 500 MHz, signals are phase-separated: green: CH₂-groups, blue: CH- and CH₃-groups

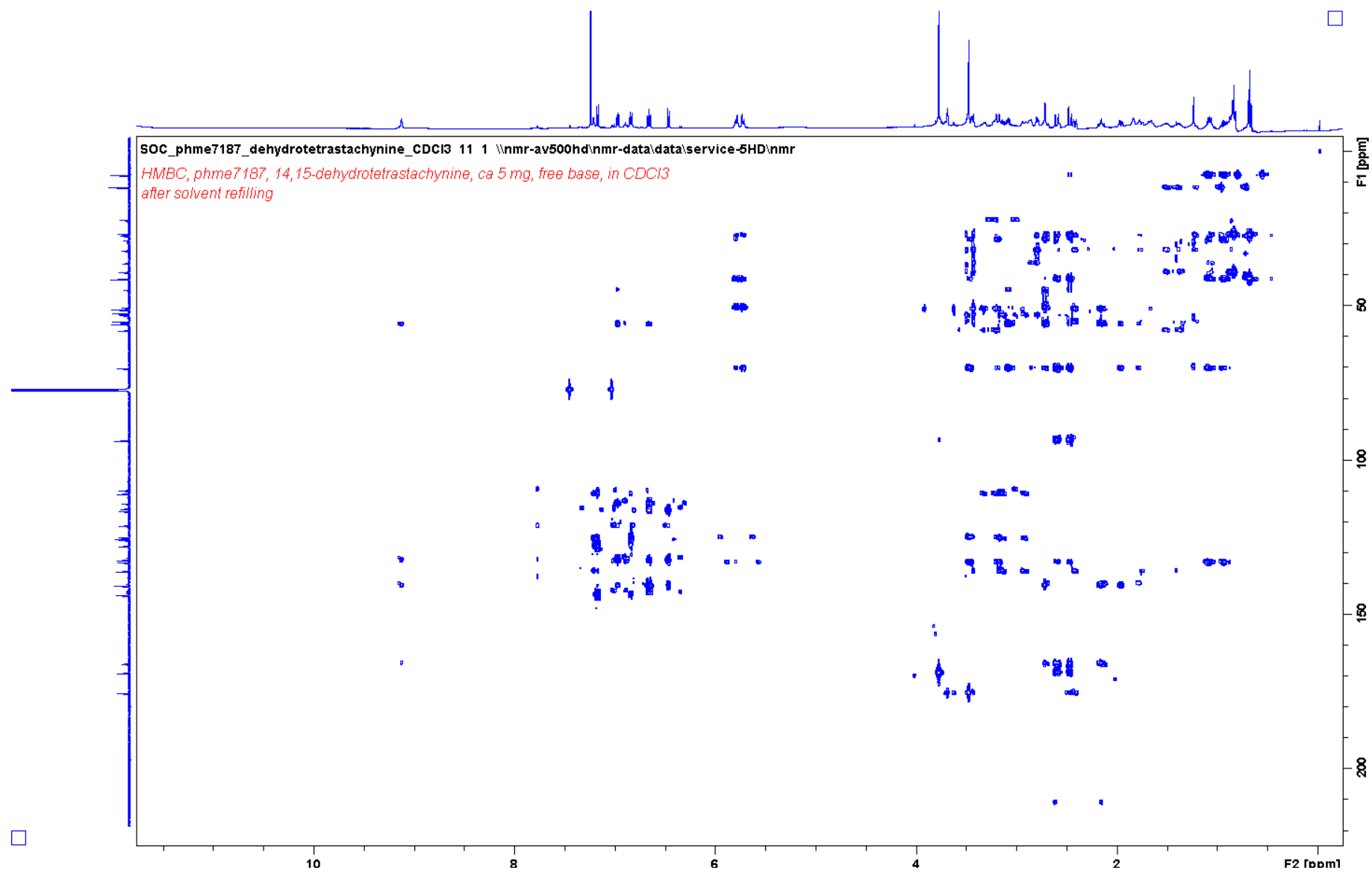


Fig. A4: HMBC-NMR spectrum of **34** in CDCl₃, 500 MHz

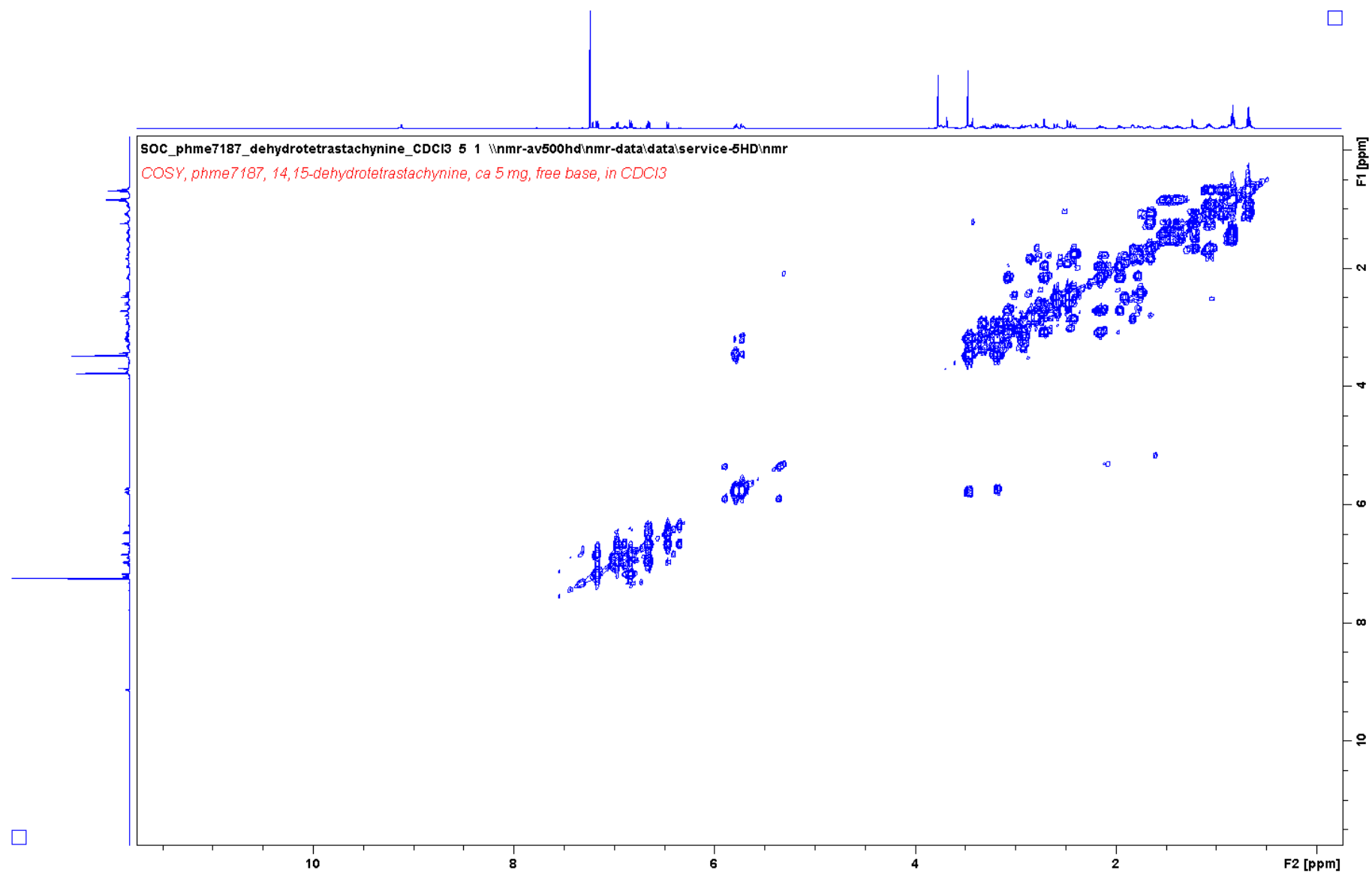


Fig. A5: ^1H - ^1H -COSY-NMR spectrum of **34** in CDCl_3 , 500 MHz

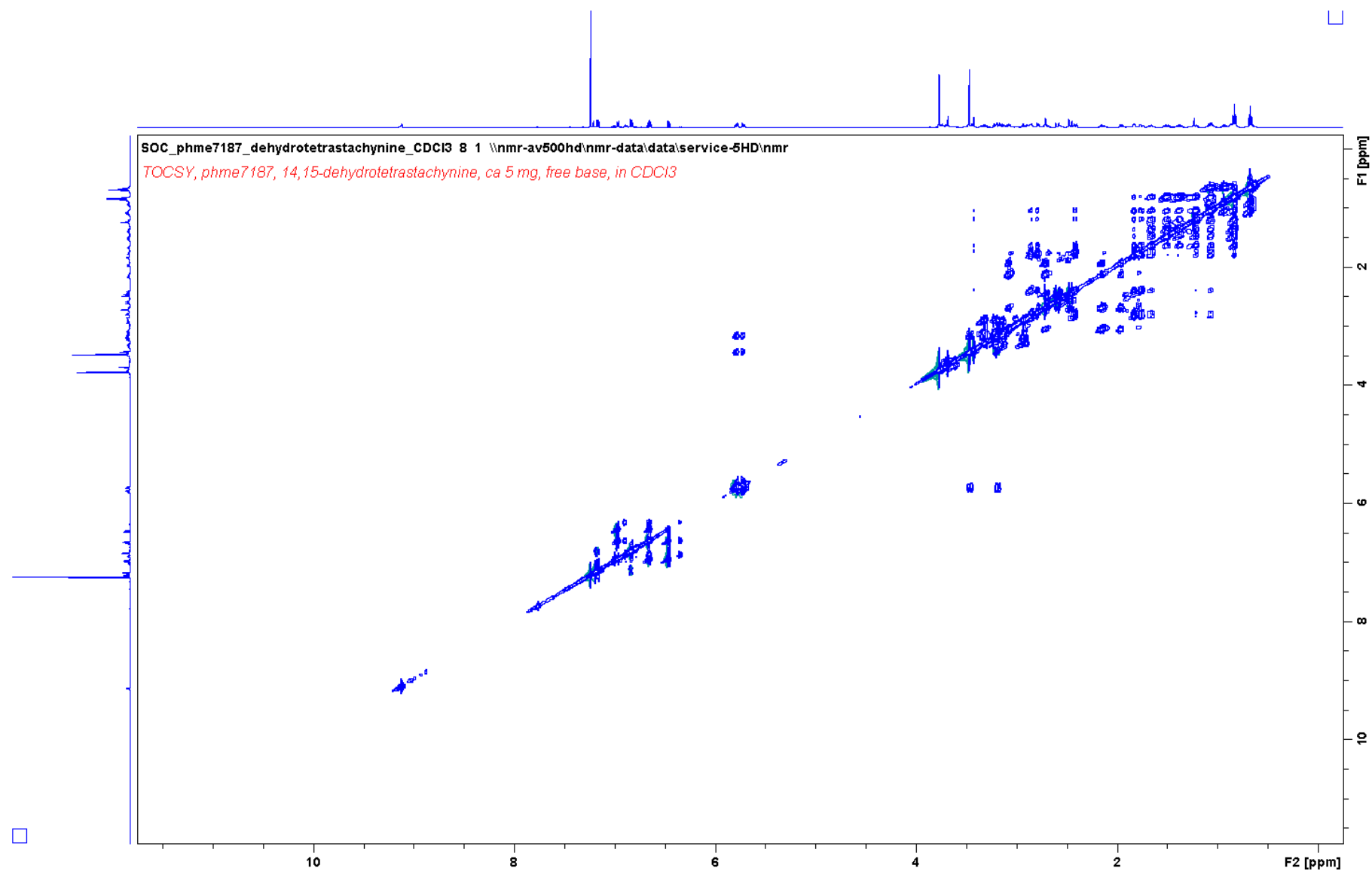


Fig. A6: ^1H - ^1H -TOCSY-NMR spectrum of **34** in CDCl_3 , 500 MHz

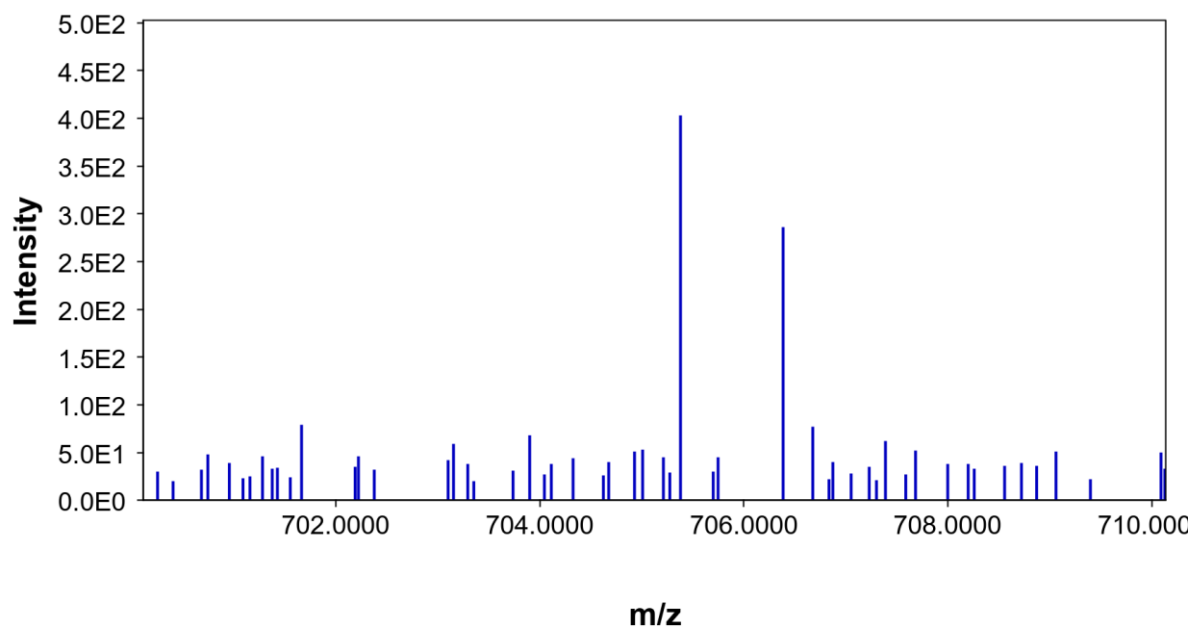


Fig. A7: MS of compound with a $t_R = 4.41$ min in leaf treated with ^{13}C -labelled **5** from feeding experiment, $m/z = 700 - 710$

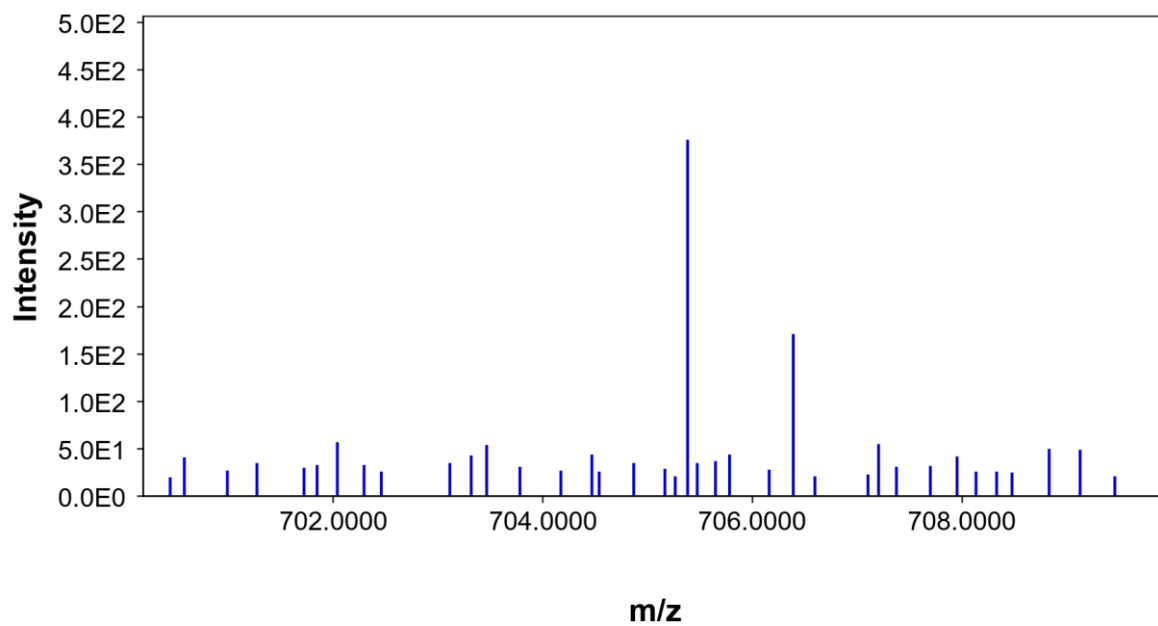


Fig. A8: MS of compound with a $t_R = 4.41$ min in control leaf of feeding experiment, $m/z = 700 - 710$

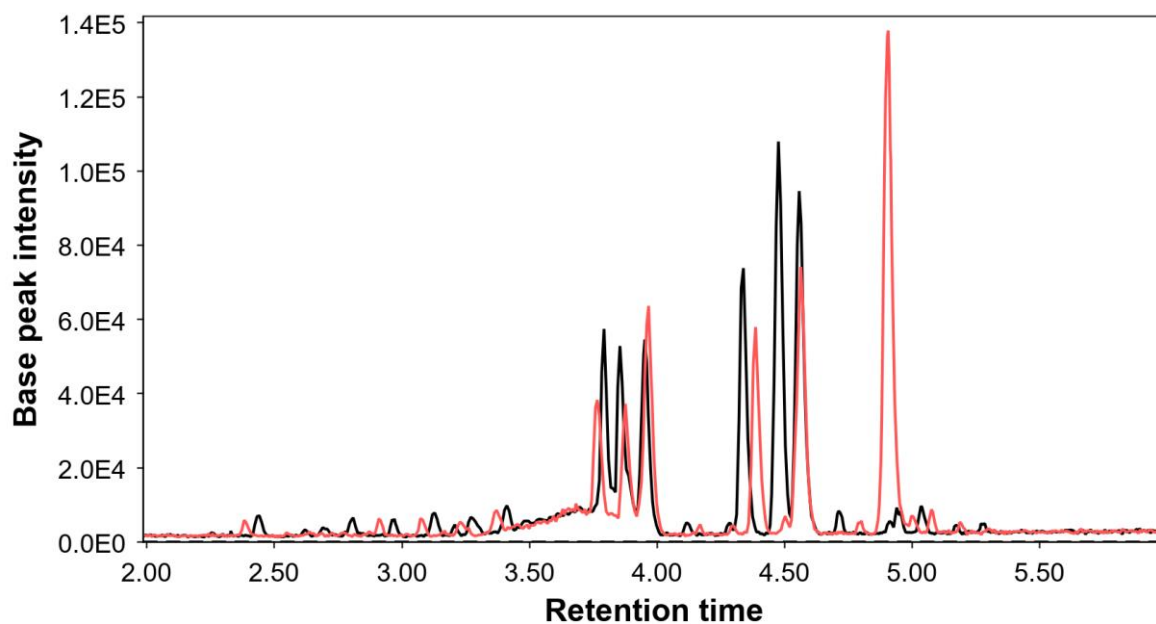


Fig. A9: comparison of samples L-AM-Tab (red) and L-BM-Cor (black) from leaf microsome assay, TIC, retention times of: **4:** 4.56 min, **5:** 4.92 min

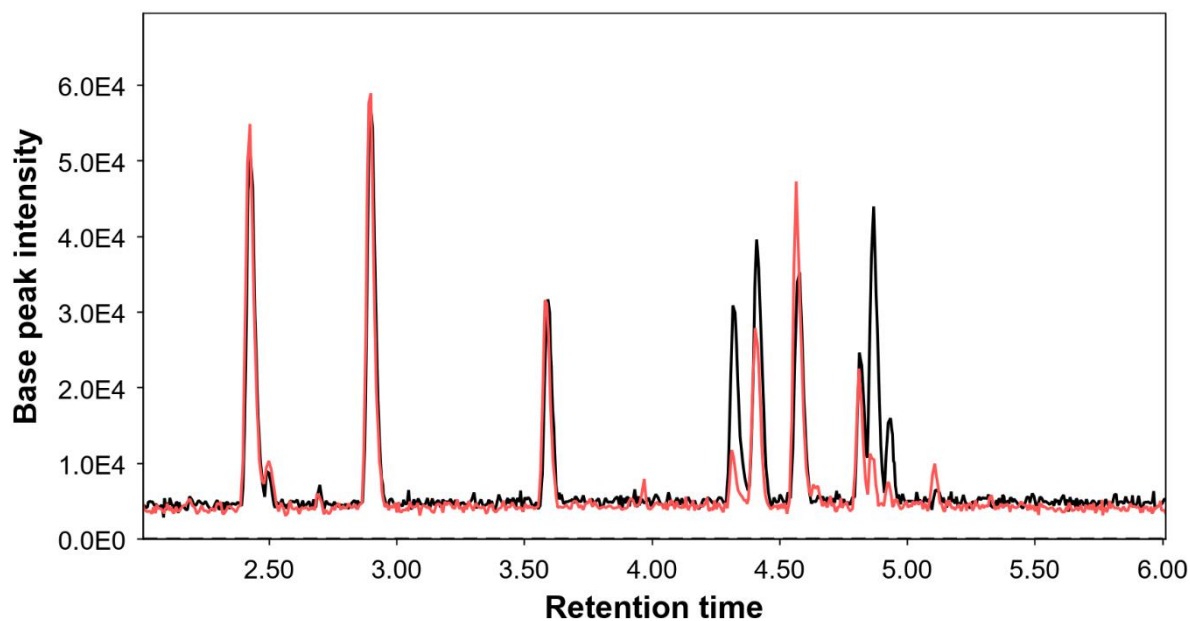


Fig. A10: comparison of samples R-AM-Tab (red) and R-AM-¹³C-Tab (black) from root microsome assay, TIC, retention time of **5:** 4.92 min

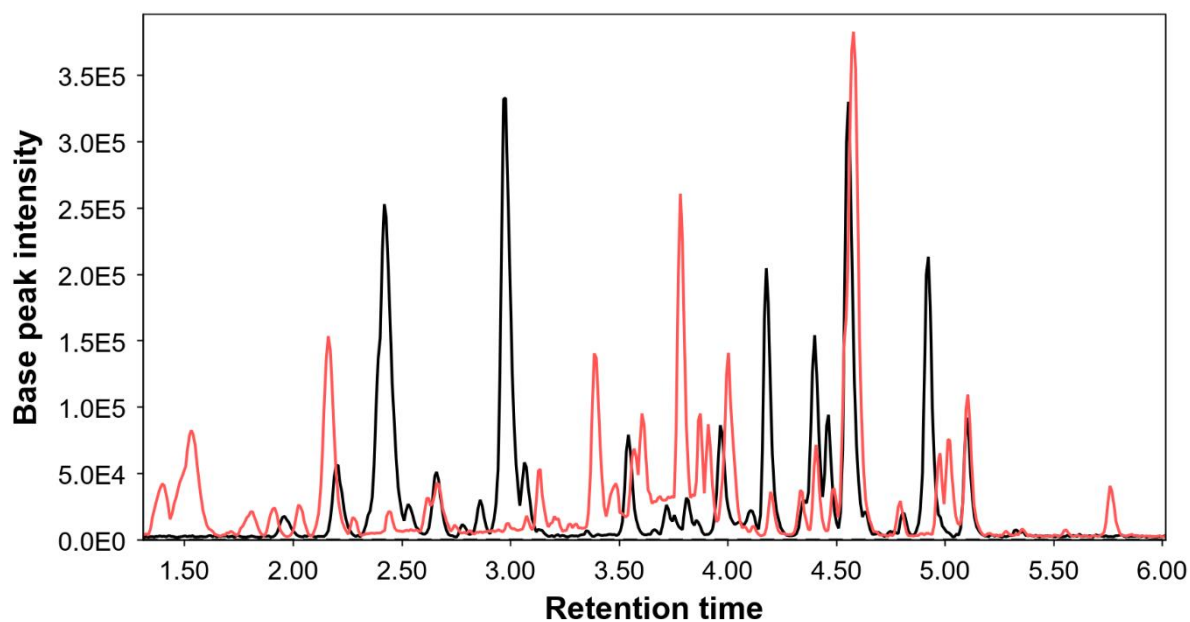


Fig. A11: comparison of metabolome of *T. donnell-smiitii* leaves (red) and roots (black), TIC, retention time of 5: 4.92 min

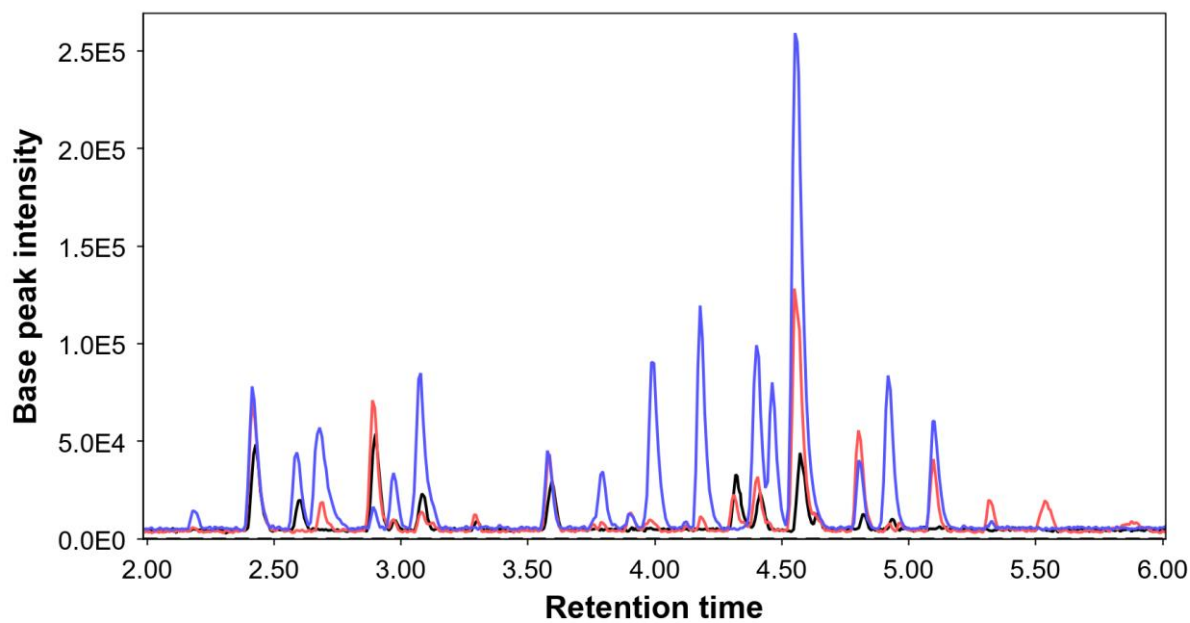


Fig. A12: comparison of samples R-BM-Tab (black) and R-BM-¹³C-tab (red) and R-BM (blue) from root-microsome assay, TIC, retention time of 5: 4.92 min

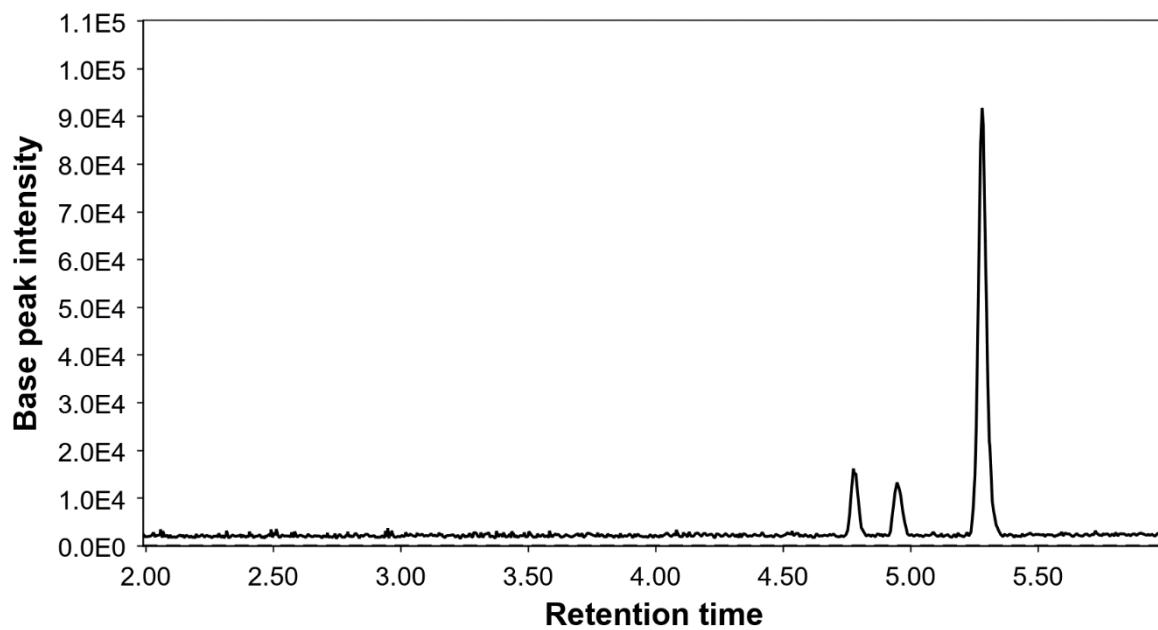


Fig. A13: chromatogram of isolated **34**, t_R of **34**: 5.33 min.

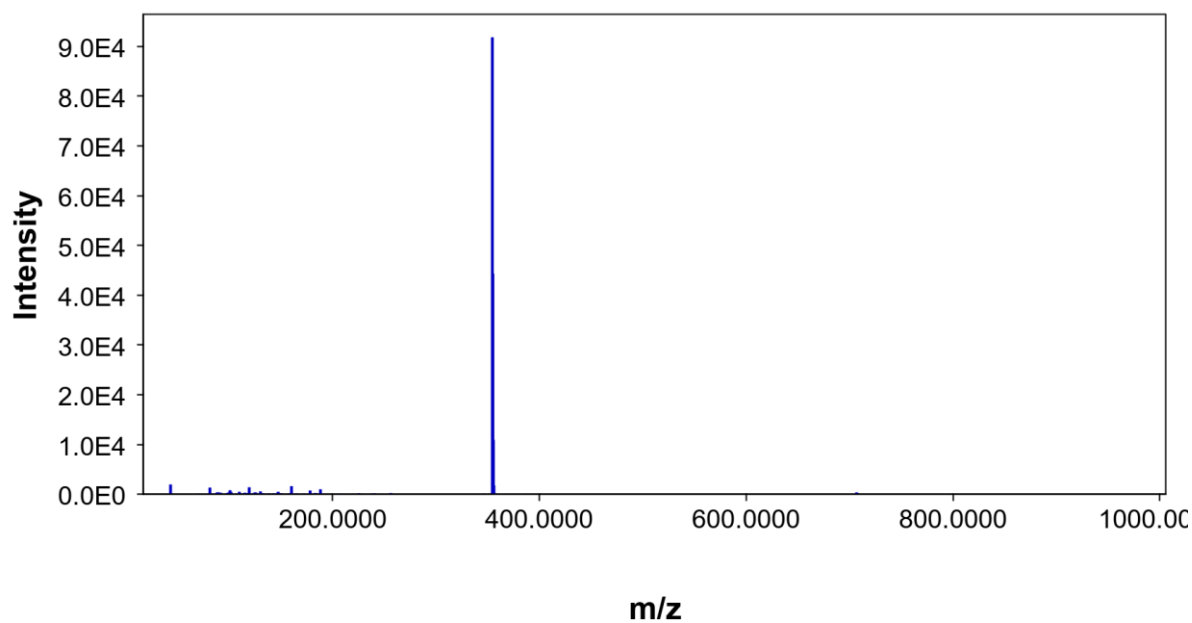


Fig. A13: mass spectrum of **34** ($t_R = 5.33$ min), $m/z([M+H]^+) = 705.37$